



ELSEVIER

Contents lists available at ScienceDirect

Deep-Sea Research II

journal homepage: www.elsevier.com/locate/dsr2

Stability of the Atlantic meridional overturning circulation and stratification in a zonally averaged ocean model: Effects of freshwater flux, Southern Ocean winds, and diapycnal diffusion

Florian Sévellec*, Alexey V. Fedorov

Department of Geology and Geophysics, Yale University, 210 Whitney Avenue, PO Box 208109, New Haven, CT 06520-8109, USA

ARTICLE INFO

Article history:

Received 12 October 2010

Accepted 12 October 2010

Keywords:

Ocean circulation

AMOC

Southern Ocean

Stability

Hysteresis

Freshwater fluxes

ABSTRACT

The Atlantic Meridional Overturning Circulation (AMOC) is a crucial component of the global climate system. In this study, using a zonally averaged ocean model, we reexamine the sensitivity of this circulation, and ocean density structure in general, to several types of external forcing. The basin of the model extends from northern high latitudes to Antarctica and includes an implicit representation of a circumpolar channel in the South, and ocean circulation is driven by surface buoyancy fluxes and wind forcing. In contrast to earlier two-dimensional studies of the AMOC, our approach involves a careful treatment of the residual mean circulation (comprising the Eulerian-mean and eddy-induced flows), which is especially important for the Southern Ocean dynamics. Using boundary conditions consistent with present-day observations the model reproduces realistic ocean stratification and meridional overturning. The structure, intensity, and stability of the overturning are then extensively studied using three control parameters: the strength of westerly wind stress over the Southern Ocean, the magnitude of freshwater fluxes imposed on the northern Atlantic, and ocean diapycnal diffusivity. In a realistic parameter range, we estimate the AMOC sensitivity to changes in the Southern Ocean winds on the order of 1 Sv per 20% increase in the wind stress. The overturning also increases with diapycnal diffusivity, but the dependence is weaker than in the absence of the winds. The model can undergo a shutdown of the overturning (subject to a hysteresis) when either the freshwater forcing gradually increases or the wind stress decreases. The hysteresis loop disappears for large values of isopycnal diffusivity. Changes in the AMOC intensity are accompanied by changes in the volume transport of the Antarctic Circumpolar Current. Specifically, the AMOC collapse leads to a strengthening of this transport. Ultimately, our calculations produce stability maps for the steady states of the meridional overturning circulation and provide a general framework that potentially can be used to compare different models, or to understand past abrupt climate changes related to reorganization of the AMOC.

© 2011 Elsevier Ltd. All rights reserved.

1. Introduction

The response of the Atlantic Meridional Overturning Circulation (AMOC) to global climate change, and its decadal to centennial variability in general, is a matter of extensive debates (e.g. IPCC AR4). To fully understand this response, to anticipate and potentially predict rapid climate changes caused by AMOC disruption, and to interpret rapid climate changes in past climate records, we need to understand the factors that control the stability of the meridional overturning in the Atlantic. This is especially important because the AMOC transports large amounts of heat and its variations have significant impacts on both global and European climates (e.g. Gagosian, 2003). The goal of this

paper is to construct a simple, yet realistic zonally averaged (latitude-depth) model of the AMOC, which can be used to explore the sensitivity of AMOC to various types of forcing in a broad parameter range.

While the history of two-dimensional ocean models is quite rich (Marotzke et al., 1988; Wright and Stocker, 1991; Drbohlav and Jin, 1998; Marchal et al., 2007, just to name a few examples), a number of important processes were left unaccounted for, including the impacts on the ocean overturning and stratification of the wind stress and dynamics in the Southern Ocean (as discussed by Marshall and Radko, 2003, 2006, for instance). Given the importance of the Southern Ocean for ocean circulation (e.g. Toggweiler and Samuels, 1995; Gnanadesikan, 1999), can those processes affect the response of a two-dimensional ocean model to external forcing, such as anomalous surface freshwater fluxes?

Over the past half-a-century or so waters in the northern Atlantic have freshened at a relatively rapid pace (Dickson et al., 2002;

* Corresponding author. Tel.: +1 203 432 1959.

E-mail address: florian.sevellec@yale.edu (F. Sévellec).

Curry et al., 2003; Curry and Mauritzen, 2005) possibly as a consequence of increase in precipitation in the subpolar gyre (Josey and Marsh, 2005). Although it is not fully clear whether these salinity changes represent decadal fluctuations or a gradual trend, this freshening can intensify if global warming enhances high-latitude precipitation or accelerates freshwater loss from high-latitude glaciers (Ekstrom et al., 2006). This is of major concern as it is believed that freshwater discharge, by affecting deep water formation in the Atlantic, played an important role in past climate changes (e.g. Broecker, 1990; Rahmstorf, 2002; Clarke et al., 2003; Alley et al., 2003). Evidence from geological records (Broecker, 1991, 2003; McManus et al., 2004; Lynch-Stieglitz et al., 2007) suggests that reorganizations of the AMOC can lead to temperature changes of several °C or more in a few decades.

A large number of modeling studies considered the consequences of such a freshening in the northern Atlantic (Rahmstorf, 1995; Manabe and Stouffer, 1995, 1999; Rind et al., 2001; Stouffer et al., 2006; Barreiro et al., 2008, and references therein). This includes studies with coupled ocean-atmosphere climate models used for making projections for future global warming. In one of those models, Stouffer et al. (2006) applied freshwater flux equivalent of 1 Sv over the northern Atlantic, which caused a shutdown of the AMOC. An ensuing large drop in sea surface temperatures in the northern Atlantic was accompanied by a substantial cooling over northern Europe. In contrast, the equatorial and southern Atlantic became warmer, leading to a global displacement of rainfall patterns in low latitudes, a southward shift of the ITCZ (also see Vellinga and Wood, 2002; Zhang and Delworth, 2005) and a deepening of the tropical thermocline (e.g. Fedorov et al., 2007; Barreiro et al., 2008).

Although these results are typically reproduced by other models, the details of the simulations such as the amount of freshwater needed for the collapse of the AMOC, the magnitude of climatic impacts, or the role of the winds over the Southern Ocean vary from one model to the next. As a result, the 21st-century projections for the AMOC summarized in the IPCC AR4 reveal a strong discrepancy between coupled models (IPCC, 2007). These issues bring about several important questions: How do we test the models? Which factors determine the sensitivity of the AMOC to freshwater and other types of forcing in a given model? What is the relative importance of different processes in bringing deep water back to the surface? To answer these questions we need to look at what determines ocean density structure and the properties of ocean meridional overturning.

The ocean circulation in the Atlantic has several components associated with different water masses (Fig. 1). The AMOC is largely defined through the formation of the North Atlantic Deep Water (NADW), which forms in the northern Atlantic, spreads southward, and upwells either in the Southern Ocean or in the regions of enhanced mixing throughout the global ocean. The Antarctic Bottom Water (AABW) is formed near the Antarctic coast and then fills the ocean abyss (except in the high latitudes of the North Atlantic). This water is brought back to the surface with the Southern Ocean upwelling while being mixed with the NADW. This process contributes to the formation of the Antarctic Intermediate Water (AAIW) that sinks to about 1000 m depth and fills intermediate depths in the ocean. The upper ocean overturning circulation – the shallow subtropical cells (e.g. McCreary and Lu, 1994; Boccaletti et al., 2004; Fedorov et al., 2004)—occupies the tropics and subtropics. Although this is very much a simplified picture of the observed three-dimensional circulation (e.g. Talley et al., 2011), it does describe the most important components of the overturning that our latitude-depth model will strive to reproduce. Note that while we refer to this circulation as the AMOC in this paper, it actually contains all the major

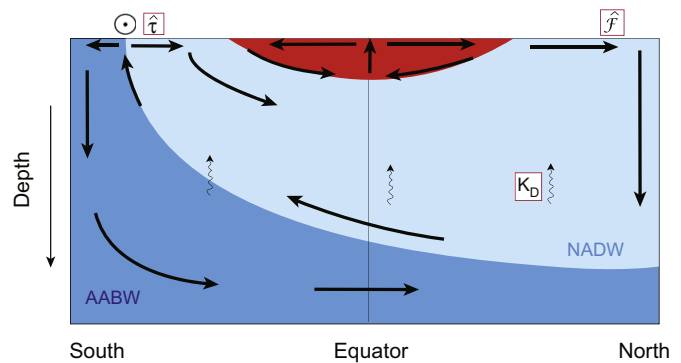


Fig. 1. An idealized schematic of the ocean Atlantic Meridional Overturning Circulation. The overturning has several major components or cells: The first component (light blue) is associated with the formation of deep water in the northern Atlantic, from where waters subduct, travel southward, and then return to the surface in the Southern Ocean (wind-driven upwelling) or elsewhere (turbulent mixing, wavy arrows). Another component (dark blue) consists of bottom circulation in which waters sink off the coast of Antarctica, travel northward, and then join the deep water to upwell at the Antarctic polar front. The upper ocean overturning (red) consists of equatorial upwelling, poleward Ekman drift, and subduction in the subtropics with a return flow in the upper 200–300 m. The surface Ekman flow, and western boundary currents such as the Gulfstream and the Kuroshio current (not shown), connect the upper and deep ocean circulations. The main control parameters used in this study are freshwater flux anomaly \hat{F} , the Southern Ocean wind stress anomaly $\hat{\tau}$, and diapycnal diffusivity K_D . Modified after Barreiro et al. (2008) (For interpretation of the references to color in this figure legend, the reader is referred to the web version of this article.)

elements of the global meridional overturning circulation, including the contribution of the Southern Ocean.

From the theoretical point of view this circulation requires an external source of mechanical energy in order to bring cold waters back to the surface. In contrast to the atmosphere, the differential heating and cooling of the ocean cannot provide this energy in accordance with the Sandström theorem (in the limit of a non-diffusive fluid, an overturning circulation cannot be sustained if the ocean is heated at a higher geopotential height than cooling). In the ocean there exist two major sources of mechanical energy—winds and internal wave breaking (e.g. Wunsch and Ferrari, 2004). In our zonally averaged model these two sources will be represented by diapycnal diffusion and prescribed wind-driven Ekman flow in the upper layer of the model ocean (winds over the Southern Ocean will be particularly important). Thus, unlike many previous two-dimensional models, our model will combine two complementary visions for the ocean abyssal circulation and stratification—one based on diapycnal mixing (Stommel, 1958; Stommel and Arons, 1960a,b) and the other reliant on wind forcing in the Southern Ocean (Toggweiler and Samuels, 1995; Gnanadesikan, 1999; Gnanadesikan et al., 2007; Hirabara et al., 2007). Also unlike earlier models, our model will incorporate the effect of ocean eddies as described by the Gent-McWilliams parameterization (Gent and McWilliams, 1990), which is essential in the region of the Antarctic Circumpolar Current (ACC).

The stability of the overturning circulation subject to a freshwater forcing has been a subject of numerous studies, starting with a box model by Stommel (1961) who showed the existence of multiple-equilibria in the system with a bistable regime. That is, a regime with two types of stable steady state solutions—strong circulation corresponding to active AMOC (the on-state) and weak circulation with a collapsed AMOC (the off-state). These results were confirmed by direct integrations of coarse resolution GCMs (Marotzke, 1991; Marotzke and Willebrand, 1991; Weaver and Sarachik, 1991; Weaver et al., 1991). Weaver et al. (1993) related the bistable regime to the role of freshwater fluxes in setting ocean stratification. Further, the AMOC multiple-equilibria have been studied in zonally averaged models (Stocker and

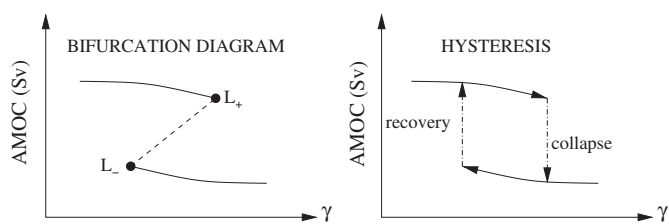


Fig. 2. (Left) A typical bifurcation diagram with two bifurcation points labeled L_- and L_+ . Solid and dashed lines indicate the branches of solutions corresponding to stable and unstable steady states of the system, respectively. (Right) An example of hysteresis behavior in the system when a control parameter (γ) gradually increases but then returns to its initial values. The direction of changes along the upper and lower branches of the hysteresis loop is shown by the arrows. At the bifurcation points the solution jumps from one type of stable steady state to the other. Modified after Dijkstra (2007).

Mysak, 1992; Schmittner and Weaver, 2001; Ganopolski and Rahmstorf, 2001), ocean GCMs (Rahmstorf, 2000; Hofmann and Rahmstorf, 2009; Prange et al., 2003; Nof et al., 2007), and intermediate-complexity coupled models (Rahmstorf et al., 2005). Similarly, continuation techniques are able to find AMOC steady states in ocean GCMs without explicit time integrations (e.g. Weijer et al., 2003; Dijkstra and Weijer, 2003).

The aforementioned studies imply or directly show a hysteresis behavior of the AMOC, linked to the bistable regime in the system (Fig. 2, modified after Dijkstra, 2007). However, the sensitivity of the hysteresis loop to ocean model parameters is still being debated. For example, Prange et al. (2003) and Nof et al. (2007) suggested that the size of the hysteresis loop diminished when the model vertical diffusivity was decreased—a result which does not necessarily agree with other studies.

Whether the hysteresis and bistable regime exist in high-resolution comprehensive coupled GCMs also remains unclear. All coupled models show a shutdown or a partial collapse of the AMOC when this circulation is subjected to a sufficient freshwater forcing in “hosing” experiments. However, when the forcing is removed many models recover the full strength of the AMOC. In contrast, a GFDL coupled model used by Manabe and Stouffer (1999) seemingly had a stable state with inactive AMOC (this conclusion was based on very few calculations with a coarse resolution). In their model the bistable regime disappeared when the model vertical diffusivity was increased, which contradicts the results of Prange et al. (2003) and Nof et al. (2007). Recently, when simulating Earth’s deglaciation between 20,000 and 15,000 yr ago with another coupled model, CCSM3, Liu et al. (2009) did not find indications of the hysteresis behavior. Thus, the problem remains unresolved, in part due to our current inability to run high-resolution coupled models for thousands of years with different sets of parameters, and also due to our lack of understanding of large-scale feedbacks between the AMOC and the atmosphere.

While idealized in many respects, zonally averaged ocean models are very efficient, which allows running hundreds or thousands of different experiments in a matter of days. In this paper, we will study the AMOC stability in such a model using key control parameters (or forcing) related to the physical phenomena we have discussed: the intensity of surface freshwater fluxes in the northern Atlantic, the strength of wind stress over the Southern Ocean, and the magnitude of diapycnal diffusivity. We will focus on how these parameters affect the strength of the AMOC and the system hysteresis. Specifically, we will investigate what factors affect the size of the hysteresis loop, he or she should distinguish between the height of the loop (the difference between the AMOC intensity in the on- and off-states) and its width (the range of control parameters for

which the bistable regime exists). As we will show, different factors can affect the two in opposite ways.

Note that in this study by the AMOC stability we mean whether (1) there exists, for a particular combination of control parameters, an AMOC on-state and (2) how close to the bifurcation point (i.e. to the AMOC shutdown) this state is. Therefore, for each model experiment we specify the relevant parameters and obtain the corresponding steady states of the ocean (one or two). This allows us to find the range of parameters (e.g. freshwater flux in the northern Atlantic) for which the AMOC is stable and outside of which the AMOC would collapse. However, here we do not consider the AMOC stability as defined, for example, in dynamical system studies (i.e. a system temporal stability with respect to small perturbations).

The structure of the paper is as follows. The zonally averaged ocean model and key approximations used in the study are described in Section 2. In Section 3, we discuss the mean (reference) state produced by the model and the strategy of perturbation experiments. Section 4 combines the results on the sensitivity of the AMOC to the main control parameters: the freshening of the North Atlantic, the wind stress over the Southern Ocean, and the diapycnal diffusivity. This section also discusses changes in the hysteresis behavior and the role of isopycnal diffusion. Major conclusions from the study are drawn in Section 5.

2. Ocean model

2.1. Model equations and configuration

The two-dimensional model used for this study is an extension of the latitude-depth model of ocean meridional circulation by Sévellec et al. (2006), which here will include the effects of surface winds and ocean eddies. The model equations are based on the zonally averaged planetary geostrophic equations in Cartesian coordinates, with a number of important dynamical approximations and parameterizations.

The main difficulty of any two-dimensional model of this kind is how to represent the geostrophic meridional flow when the zonal density gradient is not known. A number of authors (e.g. Marotzke et al., 1988; Wright and Stocker, 1991; Wright et al., 1995, 1998; Sakai and Peltier, 1995) developed different parameterizations for this meridional flow with various degrees of sophistication and detail. Our approach here is to decompose the flow felt by the tracers (temperature and salinity) into three major components: “thermohaline”, wind-driven and eddy-induced (the first two components comprise the Eulerian-mean flow):

$$v = -\frac{1}{\varepsilon\rho_0}\partial_y P + v_{\text{Wind}} + v_{\text{G\&M}}, \quad (1a)$$

$$\partial_z P = -\rho g, \quad (1b)$$

$$\partial_y v + \partial_z w = 0, \quad (1c)$$

where y is latitude, z —depth, P —pressure (hydrostatic), ρ —density (ρ_0 is the reference value), (v, w) —the zonally averaged horizontal and vertical velocities linked by the continuity equation, and g —the acceleration of gravity.

For the first (thermohaline) component in (1a) we use a simple representation that relates the flow to the meridional pressure gradient *via* a linear friction law. This is probably the simplest representation that was successfully used in a number of studies on the zonally averaged ocean circulation. Without other terms in (1a), such a representation would correspond to a frictional system where the meridional momentum dynamical balance is that between the meridional pressure gradient and horizontal friction, as in Stommel’s (1961) box model. In general, this

approximation can be justified by the fact that large-scale deep ocean flows typically go downgradient of pressure (as indicated, for example, by 2000 and 4000 dbar streamfunctions—Lynne Talley, personal communication). The choice of the linear friction coefficient $\varepsilon = 8.7 \times 10^{-4} \text{ s}^{-1}$ will give a realistic overturning of 16 Sv for the typical ocean conditions in the Atlantic.

The two other components in (1a) are ν_{Wind} —the flow velocity directly induced by the winds (for details see the next subsection) and $\nu_{\text{G\&M}}$ —the eddy-driven advection described by the turbulent closure of Gent and McWilliams (1990, GM hereafter).

$$\nu_{\text{G\&M}} = -\partial_z(K_{\text{G\&M}}S),$$

where $s = -\partial_z \rho / \partial_y \rho$ is the isopycnal slope and $K_{\text{G\&M}}$ is the Gent-McWilliams coefficient.

The only prognostic equations in the model are the equations for temperature and salinity:

$$\partial_t T = -J(\psi, T) + \partial_s(K_I \partial_s T) + \partial_n(K_D \partial_n T) + C_T + \mathcal{F}_T, \quad (2a)$$

$$\partial_t S = -J(\psi, S) + \partial_s(K_I \partial_s S) + \partial_n(K_D \partial_n S) + C_S + \mathcal{F}_S, \quad (2b)$$

where J is the Jacobian operator, ψ is the streamfunction defined as $w = \partial_y \psi$ and $v = -\partial_z \psi$. K_I and K_D are the isopycnal and diapycnal diffusivities acting along (s) and across (n) isopycnal surfaces, respectively. The forcing terms in (2a) are described by \mathcal{F} (heat and salt fluxes in the upper layer of the ocean) and C (the term due to ocean convection). When the system becomes statically unstable, convection instantaneously mixes temperature and salinity downward (conserving the ocean heat and salt content) until $\partial_z \rho = 0$.

These equations are integrated using finite differences on a uniform latitudinal grid but a non-uniform vertical grid (15 levels with the thickness ranging from 50 m at the surface to 550 m at the bottom). The no-normal-flow condition is used at the boundaries, resulting in a zero streamfunction at the boundaries, and the no-flux condition for temperature and salinity is applied at the sides and the bottom of the basin. The reference values of model parameters are given in Table 1.

A linearized equation of state for seawater is used:

$$\rho = \rho_0 [1 - \alpha(T - T_0) + \beta(S - S_0)], \quad (3)$$

Table 1
Parameters used in model.

n_y	28	Number of horizontal gridpoints
n_z	15	Number of levels in the vertical
H	4500 m	Ocean depth
W	5120 km	Basin zonal extent
y_0	66°S	Basin southern boundary
y_1	66°N	Basin northern boundary
K_I	$10^3 \text{ m}^2 \text{ s}^{-1}$	Isopycnal tracer diffusivity
K_D	$10^{-4} \text{ m}^2 \text{ s}^{-1}$	Diapycnal tracer diffusivity
g	9.8 m s^{-2}	Acceleration of gravity
ρ_0	1027 kg m^{-3}	Reference density for the equation of state of seawater
α	$2.2 \times 10^{-4} \text{ K}^{-1}$	Thermal expansion coefficient
β	$7.7 \times 10^{-4} \text{ psu}^{-1}$	Haline contraction coefficient
γ	$1/66 \text{ days}^{-1}$	Inverse of the temperature restoring timescale
\mathcal{F}_0	0.8 m yr^{-1}	Mean freshwater flux intensity coefficient
T_{min}^*	$-4 \text{ }^\circ\text{C}$	Minimum restoring temperature
T_{max}^*	$29 \text{ }^\circ\text{C}$	Maximum restoring temperature
\tilde{y}	2.8°	Asymmetry parameter for restoring temperature
τ_0	0.2 N m^{-2}	Mean wind stress intensity
c_{ACC}	1 or 3	Ekman transport coefficient (outside or inside the channel)
ε	8.7×10^{-4} or $\infty \text{ s}^{-1}$	Linear friction coefficient (outside or inside the channel)
ϵ	$2.3 \times 10^{-7} \text{ s}^{-1}$	Equatorial friction coefficient
$K_{\text{G\&M}}$	$10^3 \text{ m}^2 \text{ s}^{-1}$	Gent-McWilliams coefficient

where T and S are temperature and salinity (T_0 and S_0 are the reference values), α is the thermal expansion coefficient, and β is the haline contraction coefficient.

The model basin extends from the North Atlantic (66°N) to South Atlantic (66°N), which allows incorporating the most important physics of the AMOC (Fig. 1). To take into account the main source of the north–south asymmetry in the global ocean circulation, we have included a crude representation of the Southern Ocean circumpolar channel with the Drake Passage, which extends here from 62°S to 40°S and is 2500 m deep. In this passage, periodic boundary conditions would require a vanishing east–west pressure difference, and thus the dynamical equation (1a) has to be modified. Following Paillard and Cortijo (1999), in the channel we simply set to zero the meridional velocity component due to the pressure gradient (*i.e.* set $\varepsilon \rightarrow \infty$). In addition, to take into account the greater zonal extent of the Southern Ocean compared to the rest of the Atlantic basin, the turbulent terms are increased by a factor of 3 (by multiplying the isopycnal and diapycnal diffusivities and the GM transport coefficient). This parameterization is important to achieve a realistic intensity of upwelling in the Southern Ocean.

2.2. Ocean forcing

2.2.1. Temperature and salinity

At the ocean surface we use mixed boundary conditions for temperature and salinity. We restore temperature of the top model level to a prescribed analytical profile SST^* (Fig. 3):

$$\mathcal{F}_T(y) = \gamma(\text{SST}^*(y) - \text{SST}(y)), \quad (4a)$$

and

$$\text{SST}^*(y) = (T_{\text{max}}^* - T_{\text{min}}^*) \cos(\pi(y - \tilde{y}) / (y_1 - y_0)) + T_{\text{min}}^*, \quad (4b)$$

where γ is the inverse of the relaxation time scale for Sea Surface Temperature (SST), T_{min}^* and T_{max}^* give the range of the restoring temperature, y_0 and y_1 are the positions of the ocean southern and northern boundaries respectively, and \tilde{y} introduces a latitudinal asymmetry between the Northern and the Southern hemispheres. This latter parameter makes SST^* slightly colder in the Southern hemisphere than in the Northern (Fig. 3). The temperature restoring allows for a negative feedback between SSTs and heat fluxes (if surface temperature becomes too cold, there will be a positive heat flux going into the ocean).

To constrain salinity, at the surface we apply a prescribed salt flux:

$$\mathcal{F}_S(y) = -\frac{S_0}{h} \mathcal{F}(y), \quad (5a)$$

and

$$\mathcal{F}(y) = -\mathcal{F}_0 \sin(4\pi(|y| - y_0) / (y_1 - y_0)), \quad (5b)$$

where \mathcal{F} is the freshwater flux (a function of latitude), \mathcal{F}_0 —its amplitude, S_0 —the reference salinity, and h —the depth of the first level of the model.

2.2.2. Wind stress

The shape of zonal wind stress at the ocean surface is given by the following expression:

$$\tau = -\tau_0 \sin(3\pi y / (y_1 - y_0)) + \sin(5\pi y / (y_1 - y_0)) c_n, \quad (6)$$

where τ_0 is a wind stress intensity coefficient and c_n is a normalizing factor. For the choice of $c_n = 1.857$, τ_0 gives the maximal value of τ .

The term ν_{Wind} represents the direct effect of winds on ocean circulation in (1a). This velocity correction consists of the

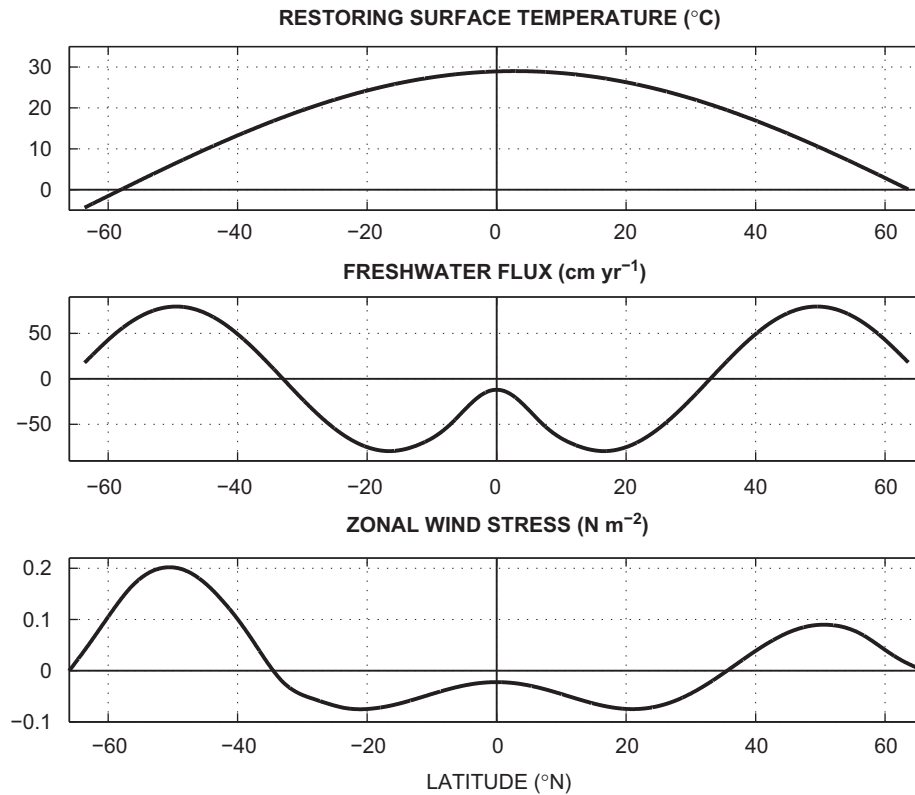


Fig. 3. The three forcing terms used as the boundary conditions at the ocean surface to obtain the model reference state: (top) the restoring Sea Surface Temperature (SST*); (middle) imposed freshwater flux; (bottom) imposed surface wind stress.

meridional Ekman flow induced by wind stress in the top layer of the model and a compensating return flow in the ocean below. The return flow is necessary to satisfy the baroclinicity condition (equivalent of mass conservation in a latitude–depth model).

The Ekman velocity is calculated as proportional to Ekman transport in the first model level:

$$v_{\text{Ek}} = c_{\text{ACC}} \frac{f}{h\rho_0(f^2 + \epsilon^2)} \tau, \quad (7)$$

where f is the Coriolis parameter (s^{-1}) and ϵ is the equatorial friction coefficient (set to $2.3 \times 10^{-7} \text{ s}^{-1}$), which keeps Ekman transport finite at the equator where $f=0$. c_{ACC} is a coefficient equal to 1 everywhere except in the circumpolar channel, where it is set to 3 to represent the greater zonal extent of the Southern Ocean as compared to the width of the Atlantic. Amplifying c_{ACC} in the channel increases Ekman transport, which is necessary to reproduce a realistic Deacon cell.

In the ocean three-dimensional dynamics, the horizontal convergence and divergence of Ekman transport induce a vertical flow at the base of the Ekman layer which, in agreement with the classical theories of Sverdrup (1947), Stommel (1948) and Munk (1950), drives ocean circulation that can be decomposed into horizontal gyre circulation and meridional overturning. The gyre circulation cannot be explicitly reproduced in a zonally averaged model because of the compensation between the interior flow and the western boundary current. However, the wind-driven meridional overturning can be reproduced by imposing the relatively shallow “return” flow to compensate for Ekman transport. We use a simple representation for this flow in which horizontal velocity decays exponentially with depth and the total integrated transport in each location is exactly equal to the local Ekman transport. The depth scale of the return flow (h_{Wind})

follows the scaling of Vallis (2006):

$$h_{\text{Wind}} = \left(\frac{f^3 W_{\text{Ek}}}{\beta_f^2 N^2} \right)^{1/3}, \quad (8)$$

where W_{Ek} is the vertical velocity induced at the bottom of the Ekman layer through nondivergence relation with the horizontal Ekman velocity (v_{Ek}), $\beta_f = d_y f$ —the gradient of planetary vorticity, and N —the buoyancy frequency.

An important assumption for deriving the scaling in (8) is that the $U \simeq V$; however, in the circumpolar channel, due to the absence of zonal boundaries, typically $U \gg V$. This would imply that $h_{\text{Wind}} \rightarrow \infty$ in the channel, and the return flow would occupy the whole depth of the ocean. In our model, we simply set h_{Wind} to the depth of the Drake Passage (2500 m), which produces a return flow similar to that in comprehensive ocean GCMs (Griffies et al., 2009).

3. Numerical experiments

3.1. The ocean reference state

Integrating the model numerically with standard boundary conditions gives the reference mean state of the ocean (to obtain steady solutions we typically continue calculations for 5000 yr). The ocean vertical stratification for the reference state is greatest in the upper 1000 m of the ocean and both temperature and salinity are important contributors to the density field (Fig. 4). Such important features of the ocean as the low-latitude warm pool and subtropical maxima in salinity are clearly evident—they reflect both ocean dynamics and surface boundary conditions in the model.

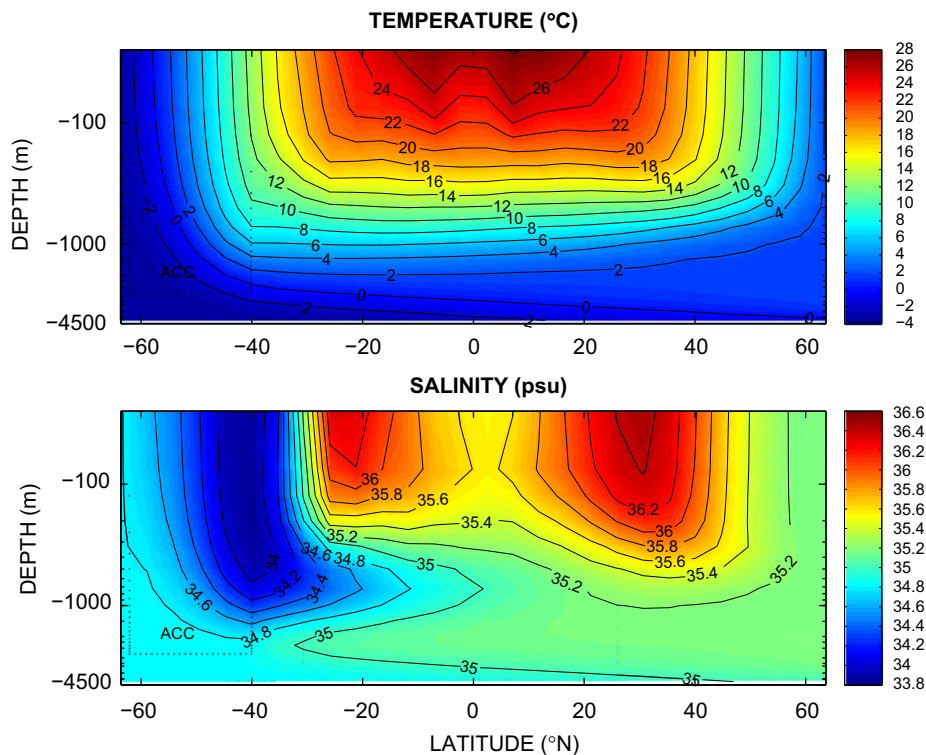


Fig. 4. (Top) thermal and (bottom) salinity fields for the on-state of the AMOC (see Fig. 5) and ocean reference conditions. Obtained by integrating the model equations with reference boundary conditions until a steady state is reached. Note several characteristic features of the modeled ocean: the low-latitude warm pool, the subtropical salinity maxima, the tongue of relatively fresh intermediate water that originates at about 40°S and then spreads northward at about 1000 m depth, and bottom water that forms near the southern boundary of the basin. The vertical scale is stretched near the surface.

In the model results we can clearly define three types of water masses filling the Atlantic: The AAIW is a relatively warm and fresh water that subsducts at around 40°S. The NADW, relatively cold and salty, is formed at the northern boundary of the Atlantic. The AABW is the coldest but relatively fresh water that originates at the southern boundary of the Atlantic.

The Eulerian-mean streamfunction, based on the thermohaline and wind-driven components of the velocity, reveals major elements of the ocean meridional overturning circulation (Fig. 5, top). The circulation is dominated by a clockwise cell that originates in the Northern hemisphere, penetrates to about 3000 m, and is most intense near the surface and along the northern boundary of the basin. In the abyssal ocean (below 3000 m) the second, counter-clockwise cell is evident. At the location of the circumpolar channel there occurs another intense clockwise cell—the Deacon cell (e.g. Speer et al., 2000). In low latitudes, there is a signature of the wind-driven shallow subtropical cells in the upper ocean.

The quasi-Lagrangian streamfunction, obtained by adding the eddy-driven contribution to the Eulerian component, shows the residual mean circulation (e.g. Marshall and Radko, 2003, 2006) that describes the actual transport of water masses and tracers in the basin (Fig. 5, bottom panel). As expected, in such a representation of the flow, the Deacon cell vanishes, and the separation of the circulation into two major cells (one corresponding to the NADW and the other to AABW) becomes even more apparent. The strength of the two cells for the model reference state, in the residual mean circulation, is 18 and 10 Sv, respectively. In our zonally averaged approach, these properties of the model critically depend on using GM eddy-driven advection as well as diapycnal and isopycnal diffusivities (cf. Sévellec et al., 2006 or Kamenkovich and Sarachik, 2004).

Another important feature of the circulation is the strong wind-driven upwelling in the Southern Ocean. Because of the Ekman transport divergence and the absence of zonal pressure

gradients the isopycnals within the circumpolar channel can outcrop and develop a strong southward slope (thick black lines in Fig. 5). In other words, the wind forcing is able to bend the isopycnals and sustain an oceanic circulation with a higher level of potential energy than without winds. The Ekman transport convergence at about 40°S drives a downwelling to a 1000 m depth, which produces the AAIW.

In agreement with previous studies (e.g. Rahmstorf, 2006), the circulation in Fig. 5 is driven by two main processes: (1) the broad vertical diapycnal mixing that upwells the dense water from the deep ocean back to the surface and (2) the wind-driven upwelling in the Southern Ocean. As the quasi-Lagrangian streamfunction indicates, there is a near equipartition between the two processes in terms of their respective contributions to the overturning.

Further, using the slope of the isopycnal surfaces and the geostrophic balance allows us to estimate the implied transport by the ACC as long as we assume a level of no motion in the deep ocean. For the reference state our calculations give the mean zonal transport through the Drake Passage of approximately 125 Sv—a value close to observational estimates which vary between 121 Sv by Whitworth (1983) and 140 Sv by Ganachaud and Wunsch (2000).

3.2. Sensitivity calculations for different control parameters

To understand what controls the AMOC – its strength, structure and stability – we have conducted a suite of numerical experiments varying the three main control parameters:

- diapycnal diffusivity (K_D),
- intensity of anomalous freshwater flux over the northern Atlantic (\hat{x}_0),
- strength of anomalous zonal wind stress over the Southern Ocean ($\hat{\tau}_0$).

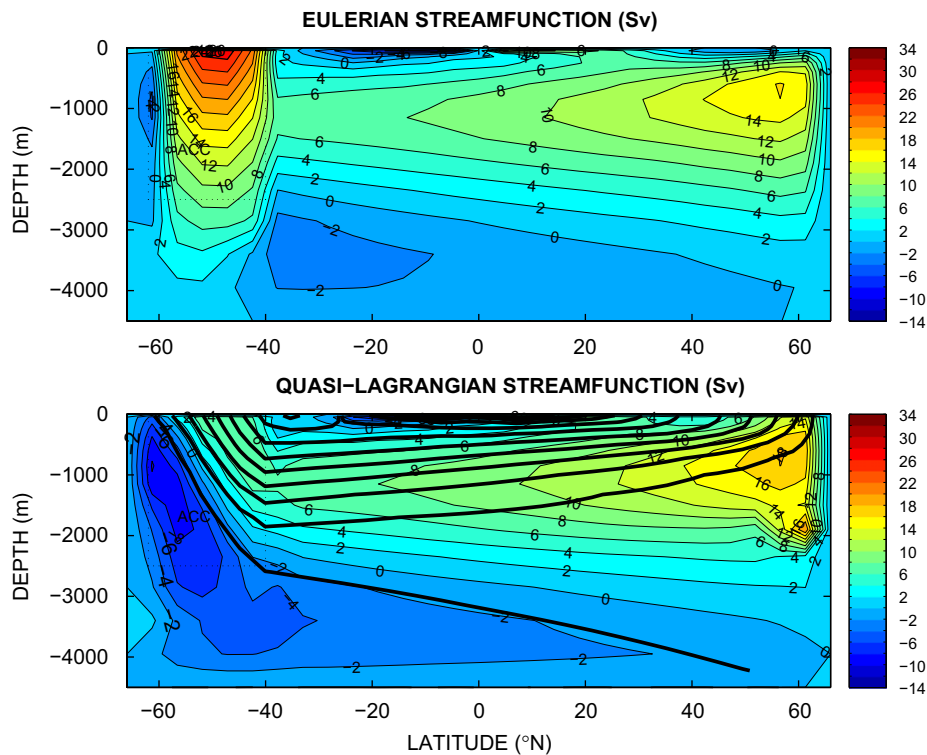


Fig. 5. The Atlantic Meridional Overturning Circulation for the reference steady state with active overturning, *i.e.* the on-state: (top) the Eulerian and (bottom) quasi-Lagrangian streamfunctions. The latter describes the mass transport in the system and is calculated as the sum of Eulerian-mean velocity and the Gent–McWilliams advection (the two terms give the residual mean circulation). In the top panel note the Deacon cell in the Southern Ocean. Thick black lines in the bottom panel correspond to ocean density surfaces. Contour intervals for the isopycnals are 0.5 kg m^{-3} ; the deepest isopycnal has potential density of 1027.5 kg m^{-3} .

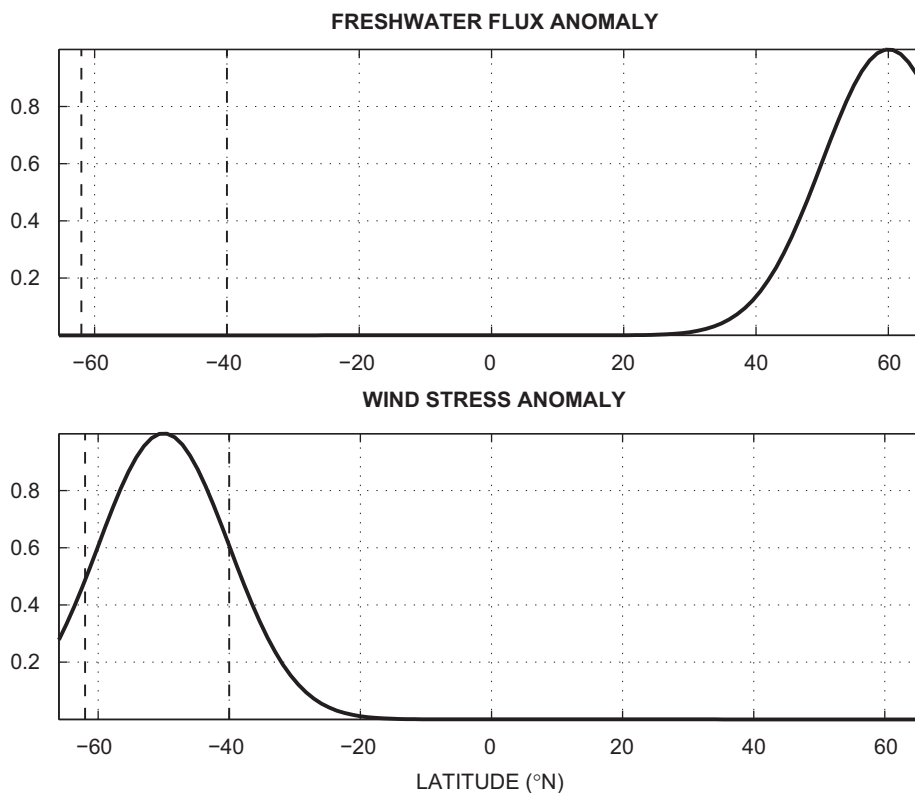


Fig. 6. The normalized latitudinal structure of (top) freshwater flux anomalies and (bottom) zonal wind stress anomalies. These profiles are multiplied by \hat{x}_0 or $\hat{\tau}_0$ and then added to the mean fields from Fig. 3. The vertical dashed lines in the Southern hemisphere indicate the meridional extent of the circumpolar channel.

A particular focus of these experiments is the AMOC intensity defined as the maximum of the overturning streamfunction in the North Atlantic between 40°N and 66°N. For each combination of parameters we obtain a new steady state of the ocean with a different AMOC intensity. Here, by the stability of the AMOC, we consider (1) whether for a particular combination of parameters there exists an on-state, and (2) how far away from the bifurcation point this state is. For example, how strong a change in freshwater forcing is needed for the AMOC shutdown. The actual strategy of the experiments is as follows.

For the first series of experiments we fix the shape of the perturbation to freshwater forcing in the northern Atlantic (\hat{F} , a Gaussian profile centered at 58°N, Fig. 6, top) and vary incrementally its magnitude (\hat{F}_0). We add this perturbation forcing to the reference freshwater flux and run the model until a new steady state is reached (each run lasts 5000 yr, but several longer integrations with a 10,000 yr duration have been performed to validate the method). For each run, the ocean state from the previous run is used as the initial condition. To follow as closely as possible the two branches of stable steady state solutions, this procedure is repeated twice—increasing \hat{F}_0 from -0.8 to $+2.4 \text{ m yr}^{-1}$ with a 0.1 m yr^{-1} increment, and then decreasing its value backward using the same increment (for the results see the next section).

Next, to explore the influence of winds over the Southern Ocean on the AMOC, we add a perturbation ($\hat{\tau}$, a Gaussian shape centered at 50°S, Fig. 6, bottom) to the reference zonal wind stress and conduct similar calculations. The magnitude of the wind stress anomaly, $\hat{\tau}_0$, is varied from 0.75 to -0.25 N m^{-2} using a somewhat non-uniform increment (with a 0.02 N m^{-2} minimum). Negative values of $\hat{\tau}_0$ correspond to easterly wind anomalies; zero values indicate the unperturbed reference wind stress.

To study the role of diapycnal diffusivity we repeat these sensitivity experiments for four values of K_D : 5×10^{-5} , 10^{-4} , 2×10^{-4} , $5 \times 10^{-4} \text{ m}^2 \text{ s}^{-1}$. Finally, some of the experiments are repeated for different values of isopycnal diffusivity (K_i).

4. Results

4.1. Two different types of ocean steady states

In agreement with previous studies, imposing a freshwater flux over the northern Atlantic weakens the ocean overturning in the model. Varying the freshwater flux and monitoring the strength of the AMOC reveals the existence of a hysteresis behavior (Fig. 7) analogous, in principle, to the results of Stommel (1961). The hysteresis implies that there are two types of stable steady states and for a range of freshwater fluxes either one is possible. In this regime, the system will reach one or the other stable steady state depending on which initial conditions were used.

The upper branch of the solutions, corresponding to a strong AMOC (the on-states), is the branch where our reference state is located (Fig. 7). Other steady solutions along this branch have properties (in terms of dynamics and ocean stratification) generally similar to the reference state shown in Figs. 4 and 5.

Steady states along the lower branch exhibit a dramatically weaker AMOC (the off-states). The formation of NADW ceases, and the Atlantic ocean becomes filled almost entirely with the AAIW and the AABW (Fig. 8). Ocean stratification for these states has undergone a strong reorganization as compared to that for the upper-branch solutions. Isopycnal surfaces have become virtually horizontal everywhere, except in the Southern Ocean. Overall, ocean stratification and overturning circulation in the off-states strongly resemble the modern Pacific.

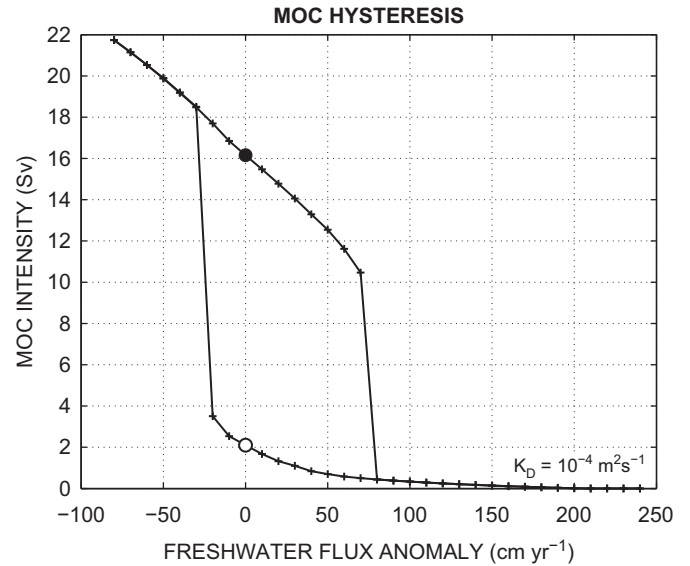


Fig. 7. The AMOC strength for the model steady states as a function of freshwater flux in the northern Atlantic. Note the hysteresis regime with two branches of steady state solutions—the upper branch (the AMOC on-states) and the lower branch (the AMOC off-states). The solid black dot along the upper branch indicates the reference solution corresponding to the ocean’s present-day conditions. The model parameter regime is such that another steady solution can exist for these conditions (indicated by an open circle on the lower branch of the hysteresis loop).

To understand some of the differences between these steady states one can consider the meridional transport of heat and freshwater for the two cases:

$$H_{TR} = W \int_{y_0}^y dy Q_{T|eq} \quad \text{where} \quad \frac{1}{h\rho_0 C_p} Q_{T|eq} = \mathcal{F}_{T|eq} = \gamma(SST^* - SST|_{eq}), \quad (9a)$$

$$F_{TR} = W \int_{y_0}^y dy \mathcal{F}, \quad (9b)$$

where W is the basin zonal extent. *A priori*, there is no reason for the $SST|_{eq}$ (Sea Surface Temperature at the steady state), and thus $Q_{T|eq}$, to be the same for both types of steady states. Therefore, using a steady state balance and expressions for the surface fluxes of heat and salt, one can compute and compare the meridional heat and freshwater transports for the two cases.

The ocean meridional heat transports for different types of steady states are quite different indeed (Figs. 9 and 10). For the active AMOC, heat transport is northward with the maximum in the North Atlantic. For the collapsed AMOC, heat transport is mainly southward with the maximum in the South Atlantic, which implies that the Northern hemisphere exports heat to the South. Thus, in agreement with previous studies (e.g. Barreiro et al., 2008), our zonally averaged model demonstrates that a shutdown of the AMOC circulation must have a significant impact on the climate associated with the reversal of heat transport by the ocean (a strong cooling of the northern Atlantic and a warming in the South). In contrast, freshwater transports remain the same since they are determined by prescribed freshwater fluxes at the surface.

To further understand processes that control the two different steady states we can split the meridional heat transport into advective and turbulent terms (Fig. 9):

$$H_{TR} = H_{TR}^{ADV} + H_{TR}^{TUR} = (H_{TR}^{TH} + H_{TR}^{WD}) + (H_{TR}^{DIFF} + H_{TR}^{GM}). \quad (10)$$

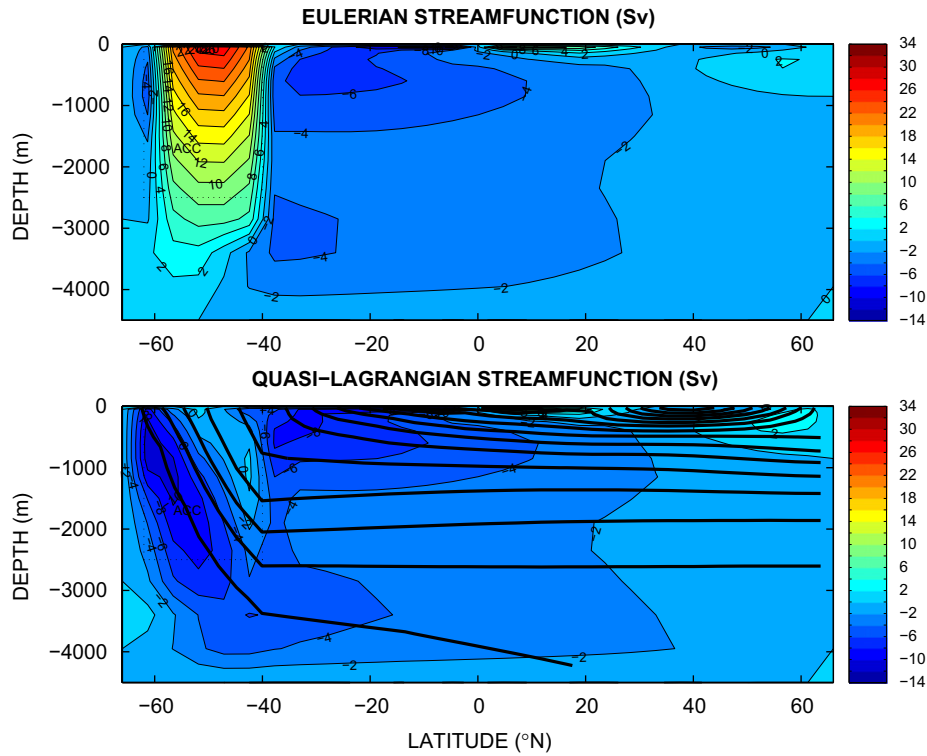


Fig. 8. As in Fig. 5, but for the second steady state and reference conditions, i.e. the AMOC off-state (corresponding to the open circle in Fig. 7). Contour intervals for the isopycnal surfaces in the bottom panel are 0.5 kg m^{-3} ; the deepest isopycnal has potential density of 1028 kg m^{-3} .

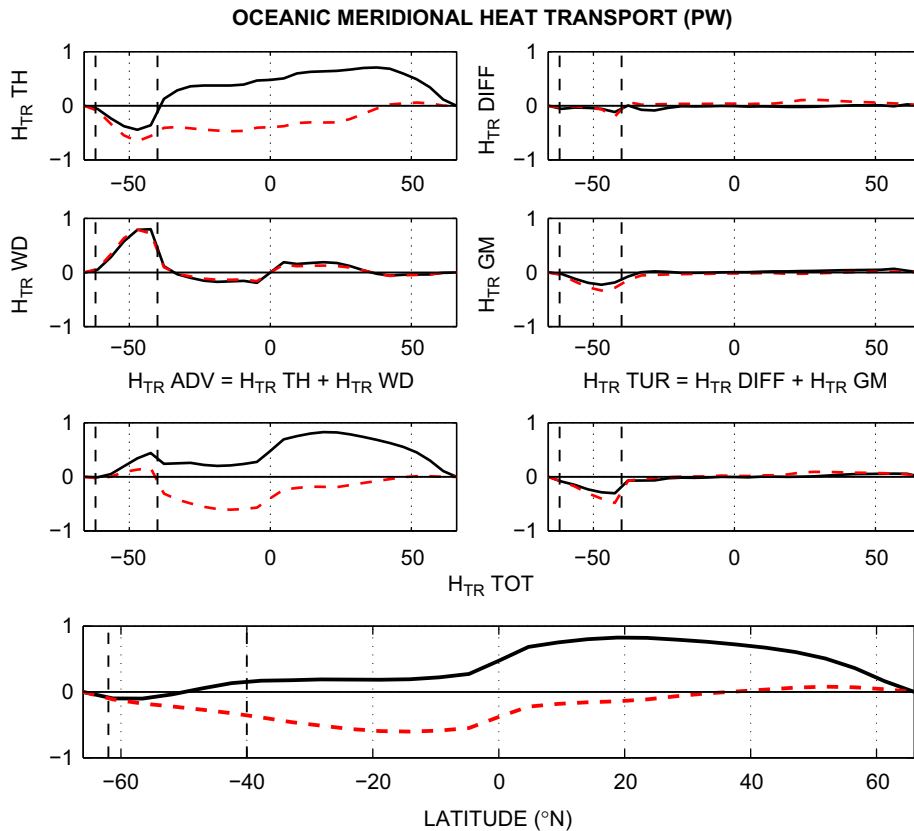


Fig. 9. Oceanic heat transport H_{TR} (bottom panel) and its components (upper panels) for the on- and off- states of the AMOC (solid black and dashed red lines, respectively). The heat transport is decomposed into two advective terms (due to the “thermohaline” and wind-driven advection—TH and WD – left top panels) and two turbulent terms (due to diffusion and the GM parameterization—DIFF and GM – right top panels). Positive values imply northward transport. The vertical dashed black lines in the Southern hemisphere indicate the meridional extent of the circumpolar channel.

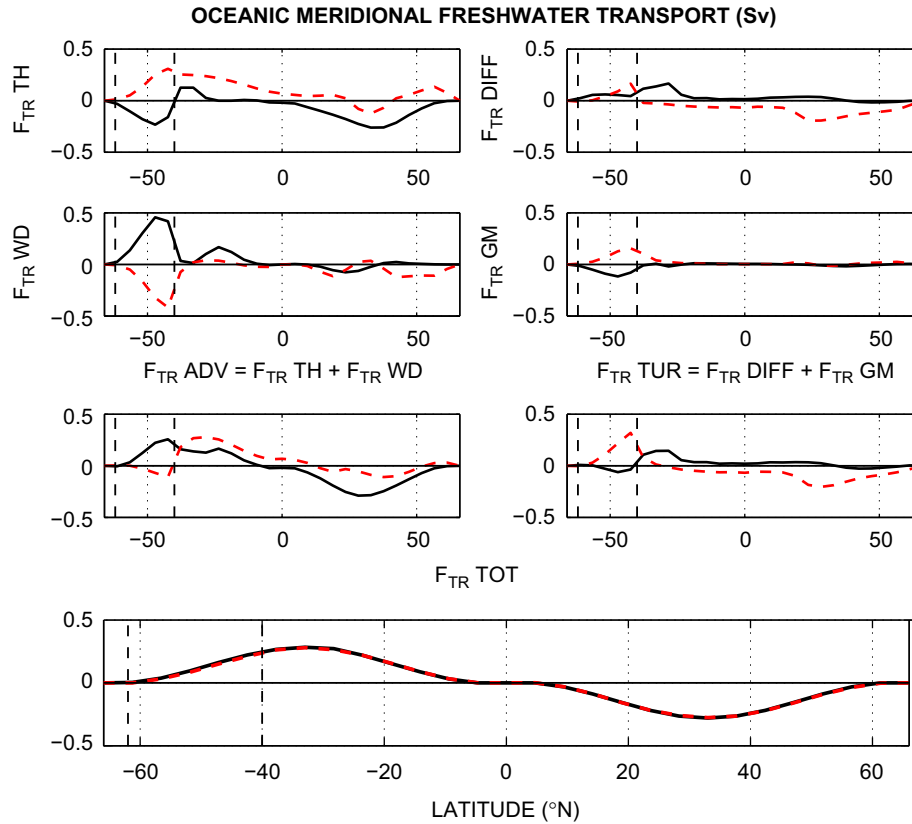


Fig. 10. As in Fig. 9 but for the ocean freshwater transport (F_{TR}). Positive values imply northward transport.

These expressions can be expressed as

$$H_{TR}^{TH} = W\rho_0 C_p \int_{-H}^0 dz v_{TH} T \quad \text{and} \quad H_{TR}^{WD} = W\rho_0 C_p \int_{-H}^0 dz v_{Wind} T,$$

$$H_{TR}^{DIF} = W\rho_0 C_p \int_{-H}^0 dz K_H \partial_y T \quad \text{and} \quad H_{TR}^{GM} = W\rho_0 C_p \int_{-H}^0 dz v_{G\&M} T,$$

where $v_{TH} = v - v_{Wind} - v_{G\&M}$ and K_H is the horizontal diffusivity – a function of K_I and K_D , and the isopycnal slope (Redi, 1982). Such decomposition reveals that for both states the “thermohaline” advection controls ocean heat transport. However, for the state with a collapsed AMOC, there is almost no heat transport reaching the northern Atlantic (north of 40°N there still occurs a very weak poleward heat transport associated with turbulent mixing in the model).

Although the meridional freshwater transport is exactly the same in both experiments (Fig. 10), splitting it into four components, as we did for the heat transport, reveals that the physical processes controlling the freshwater transport are quite different in these experiments. In the first case (on-states), freshwater is removed from the northern Atlantic by advection, in the second (off-states)—by diffusion. In the region of the Antarctic circumpolar channel, one of the main processes responsible for the transport of freshwater is the wind-driven flow. However, in the former case it moves freshwater equator-ward, in the latter—pole-ward. Since the wind stress and the penetration depth of the wind-driven return flow in the channel are fixed, this is an indication that the wind-driven flow transports different water masses. This happens because, in the absence of the AMOC, the NADW cannot reach this region anymore.

4.2. The role of different upwelling mechanisms

As discussed previously, in our ocean model there are two different types of upwelling – a broad diapycnal upwelling throughout the basin and the wind-driven upwelling in the circumpolar channel – both are important for the overturning. To investigate the relative role of these two effects we can alter either diapycnal diffusivity or the wind strength over the Southern Ocean (which would increase the slope of the isopycnals and the upward residual mean velocity).

One of the most dramatic effects we found in the model is an AMOC hysteresis that emerges when the strength of the Southern Ocean winds is varied (Fig. 11). For wind stress perturbations with roughly twice the strength of the reference wind stress, there is only one solution with a strong AMOC. Similarly, for strong negative wind perturbations, that basically wipe out all wind stress over the circumpolar channel, there exists only one state but with a weak meridional overturning. Between these two extremes, the system is bistable and both on- and off-states can exist.

Along the upper branch of steady state solutions (on-states) the AMOC intensifies with the wind stress over the Southern Ocean (Fig. 11), but some saturation occurs for stronger wind perturbations. Also, the AMOC becomes less sensitive to wind increases at larger values of diapycnal diffusivity (Fig. 12, left). This is indicative of a competition between the two effects: if diapycnal mixing is strong enough to sustain most of overturning, the relative contribution of the winds is reduced.

Not only do the winds over the Southern Ocean strengthen ocean overturning, but they also enhance the stability of the AMOC. That is, stronger winds move the bifurcation point farther from a given ocean state and increase the width of the hysteresis loop (Fig. 13). As a result, the range of the bistable regime is

broadened by the effect of the Southern ocean winds, which is opposite to the conclusion of Nof et al. (2007).

As expected, diapycnal diffusivity increases the intensity of the AMOC (Fig. 12, right). A number of different theoretical and numerical scalings for this dependence exist. Vallis (2000) used the primitive equations of motion for an idealized Atlantic basin and showed that the overturning intensity should vary as $K_D^{2/3}$ (without winds) and as $K_D^{1/2}$ (with zonal winds), where K_D is vertical diffusivity. Studies with ocean GCMs show the $K_D^{1/3}$ law (Dijkstra, 2008) and $K_D^{2/3}$ law (Zhang et al., 1999; Mignot et al., 2006). Park and Bryan (2000) showed that the AMOC volume and meridional heat transport followed roughly the $K_D^{2/3}$ law (in both z-coordinate and layered model). In a two-dimensional model Wright and Stocker (1992) observed a dependence of $K_D^{0.46}$. In our calculations this dependence was close to $K_D^{1/2}$, but this power

varied between roughly 1/3 and 2/3 depending of the parameter range.

The effect of diapycnal diffusion on the hysteresis behavior was not as straightforward in our model. For example, for the reference mean winds (with zero wind stress perturbation, Fig. 13, left), the hysteresis loop becomes larger first with increasing diapycnal diffusivity but then shrinks and virtually disappears at very large values of diffusion. The latter result is different from the conclusion of Nof et al. (2007), but tentatively agrees with that of Manabe and Stouffer (1999). The reasons for this discrepancy are currently unclear. Overall, these experiments demonstrate that the extent of the hysteresis regime is controlled by the competition between the two upwelling processes: one driven by winds in the Southern Ocean and the other driven by diapycnal mixing.

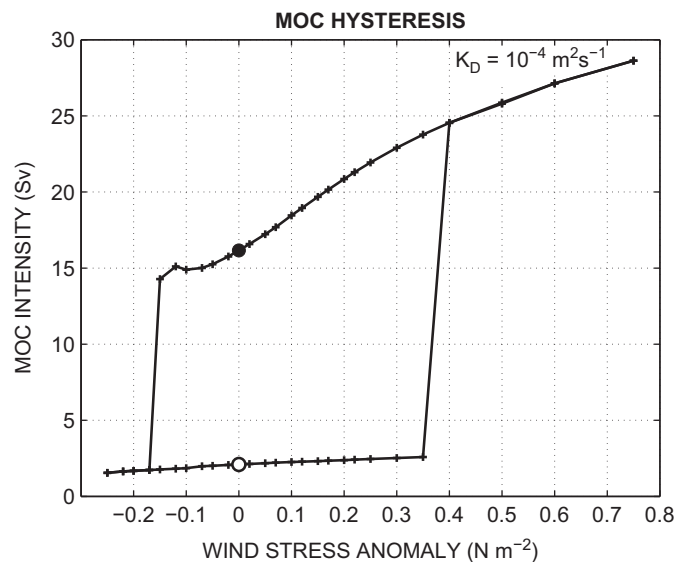


Fig. 11. AMOC intensity as a function of anomalous wind stress $\hat{\tau}_0$ in the Southern Ocean. The black dot indicates the ocean main reference state (the on-state, present-day conditions). The second reference solution, corresponding to the AMOC off-state, is shown by an open circle. The model parameter regime is such that varying wind stress in the Southern Ocean produces a hysteresis behavior.

4.3. Stability maps

To summarize some of the results of the sensitivity experiments we have generated maps of the AMOC steady states (Fig. 14). These maps show the intensity of the AMOC as a function of wind stress and freshwater flux anomalies, as well as the borderlines where the transition between the two types of stable steady state solutions occurs. Maps on the left-hand side of the figure correspond to calculations when we increase freshwater flux from one experiment to the next, whereas maps on the right-hand side correspond to experiments when we reduce the flux. Differences between the maps on the left and the right reflect the hysteresis behavior of the system.

On the whole, these maps show the competition between the effects of the Southern Ocean winds (strengthening the AMOC and broadening its stability range) and of the freshwater flux in the northern Atlantic (weakening the AMOC and then causing it to collapse). In fact, the strengthening of the winds allows the overturning circulation to exist even with weak meridional density gradients.

The experiments have been repeated for three values of diapycnal diffusivity (different rows of panels in Fig. 14). The results indicate that an increase in diapycnal diffusion does not affect too much the values of freshwater flux needed for the AMOC to collapse.

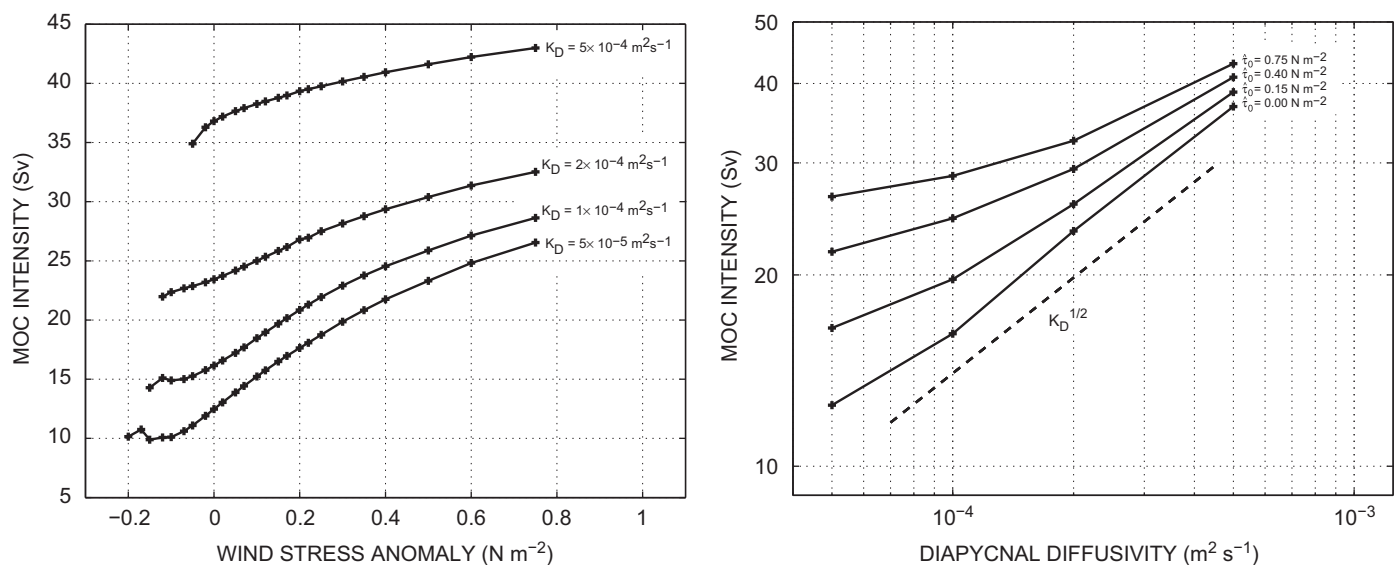


Fig. 12. (Left) AMOC intensity as a function of anomalous wind stress $\hat{\tau}_0$ in the Southern Ocean for different values of diapycnal diffusivity for the upper branch of the hysteresis plots in Fig. 11 (the AMOC on-states). (Right) AMOC intensity as a function of diapycnal diffusivity K_D for different wind stress anomalies.

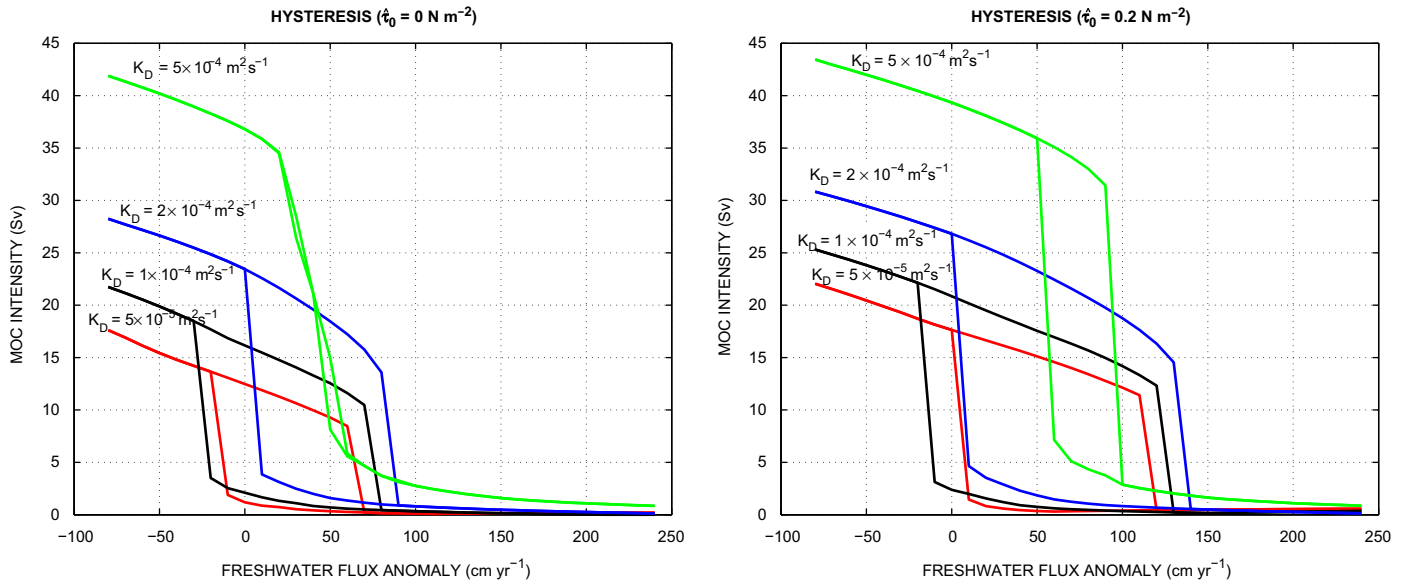


Fig. 13. AMOC hysteresis plots: as in Fig. 7 but for two different Southern Ocean wind stress anomalies (left: $\hat{\tau}_0 = 0$, right: $\hat{\tau}_0 = +0.2 \text{ N m}^{-2}$) and four different values of diapycnal diffusivity: $K_D = 5 \times 10^{-5}, 10^{-4}, 2 \times 10^{-4}, 5 \times 10^{-4} \text{ m}^2 \text{ s}^{-1}$.

In summary, the maps in (Fig. 14) show the ranges of the stable AMOC on- and off-states, and the range where either of the states is possible. By showing the boundary where the AMOC on-state would cease to exist, these maps indicate for which parameters the AMOC will collapse. As such, here we refer to these maps as the AMOC stability maps.

In particular, these maps allow us to estimate the sensitivity of the AMOC to changes in freshwater forcing in the northern Atlantic or wind stress in the Southern Ocean. We find that the sensitivity of the AMOC for the model reference state is roughly 1 Sv per 20% increase in the wind stress and -0.7 Sv for a 10 cm yr^{-1} increase in freshwater fluxes.

4.4. The effect of the isopycnal diffusion

Another important parameter of ocean models (sometimes overlooked) is isopycnal diffusivity. Here, we have conducted sensitivity experiments to investigate the role of isopycnal diffusivity (K_I) in our model. To that end, we have looked at how different ocean stable steady states are modified in response to changes in freshwater fluxes imposed on the northern Atlantic for different values of K_I (Fig. 15).

The first result of this set of experiments is a substantial decrease of the ocean overturning for larger values of isopycnal diffusivity. An order of magnitude increase in K_I reduces the overturning strength from 20 to 5 Sv (for zero freshwater flux). The second important result is a substantial decrease in the size (both width and height), and eventual disappearance of the hysteresis loop when isopycnal diffusivity increases (Fig. 15).

4.5. The ACC zonal transport

Our thorough treatment of the processes in the Southern Ocean also allows us to explore how the volume transport of the ACC depends on the main control parameters of this study. Since there are no explicit zonal dynamics in our model, the zonal velocity can be estimated from ocean stratification, or more precisely from the slope of the isopycnals in the circumpolar channel. To do so, one can use the thermal wind balance and assume that the zonal flow vanishes just below the channel. Thus

in effect, this procedure yields the ACC total transport through the Drake Passage. For our reference state, we estimate the net zonal ACC transport, calculated by integrating the zonal velocity within the channel, at 125 Sv, which agrees well with the observations within their uncertainty range (Whitworth, 1983; Peterson, 1988; Orsi et al., 1995; Ganachaud and Wunsch, 2000).

Further, we investigate how changes in the Southern Ocean winds and diapycnal diffusivity influence the magnitude of the net ACC volume transport (Fig. 16). As expected, the winds in the Southern Ocean are critical in controlling this transport—stronger winds imply a greater North–South slope of the isopycnals, a larger vertical shear of the zonal velocity and a stronger ACC. The eddy-induced southward advection (described by the GM parameterization in the model) prevents the isopycnals from becoming fully vertical and thus mediates the increase of the zonal transport through the channel. The model dependence of the ACC transport on wind stress follows closely a logarithmic law, $a + b \log(\bar{\tau}_0)$, where $\bar{\tau}_0$ is here the total magnitude of the zonal wind stress in the channel ($\approx \tau_0 + \hat{\tau}_0$), and a and b are constants. Previous studies show power laws with the power ranging from 1/2 to 1/3 (Tansley and Marshall, 2001), or a linear law (Bryden and Cunningham, 2003). Our study, using a broader range of wind stress intensity, could be a generalization of these previously derived laws.

We also find a moderate dependence of the ACC transport on diapycnal diffusivity. For the standard wind stress, increasing diapycnal diffusivity from 5×10^{-5} to $5 \times 10^{-4} \text{ m}^2 \text{ s}^{-1}$ raises the ACC transport by 20 Sv or roughly 16% (for stronger Southern Ocean winds this sensitivity becomes weaker). The mechanism of this increase is related to the deepening of the ocean thermocline throughout the ocean and, especially, in the Southern hemisphere when diffusivity goes up, which increases the slope of the isopycnals in the circumpolar channel.

Next, investigating the effect of freshwater flux in the northern Atlantic gives two important results (Fig. 17). Imposing the freshwater flux increases the net ACC transport. Moreover, it turns out that the ACC can have two different states corresponding to different states of the overturning (*i.e.* the AMOC on- and off-states). For zero freshwater anomalies in the model, the ACC volume transports for the two states are 125 and 143 Sv, respectively (the former value corresponds to our present-day conditions).

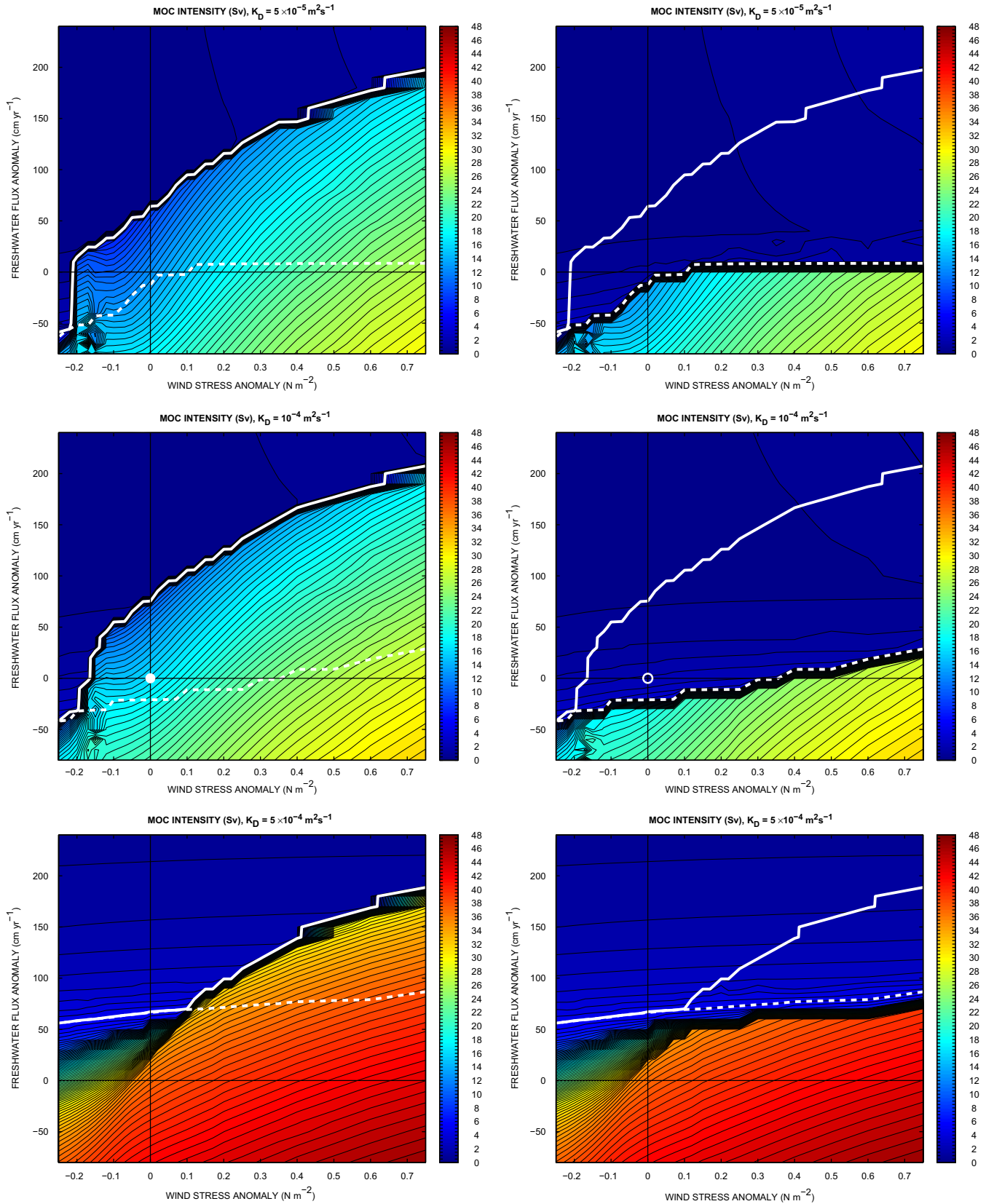


Fig. 14. Stability maps showing AMOC intensity (in Sv) for model stable steady states as a function of anomalous freshwater flux \hat{F}_0 in the northern Atlantic and wind stress anomaly $\hat{\tau}_0$ in the Southern Ocean. The left-side column: states obtained when increasing freshwater flux. The right-side column: decreasing freshwater flux. The dots indicate ocean states for the reference ocean conditions (cf. Figs. 7 and 11). The white lines indicate the boundaries of the bistable regime: for the parameters above the solid line the AMOC collapses; below the dashed line the AMOC off-states do not exist. The three rows of panels correspond to different diapycnal diffusivities (from top to bottom: $K_D = 5 \times 10^{-5}, 10^{-4}, 5 \times 10^{-4} \text{ m}^2 \text{ s}^{-1}$). Contour intervals for AMOC intensity are 0.5 Sv.

The ocean off-state has a greater ACC transport because of a larger meridional density gradient across the circumpolar channel below 1000 m and hence a stronger vertical shear there (Fig. 18), which also implies stronger zonal velocities at depths (Fig. 19). These effects are related to the deepening of the thermocline outside the channel and the corresponding increase in the slope of the isopycnals in the channel for the off-state. It is interesting, however, that surface velocities are slightly lower for the off-state, because of a weaker shear in the upper ocean.

The deepening of the ocean thermocline and the resultant adjustment of the slope of the isopycnal surfaces within the channel also explain the increase of the ACC net volume transport when freshwater flux in the northern Atlantic or diapycnal diffusivity is increased.

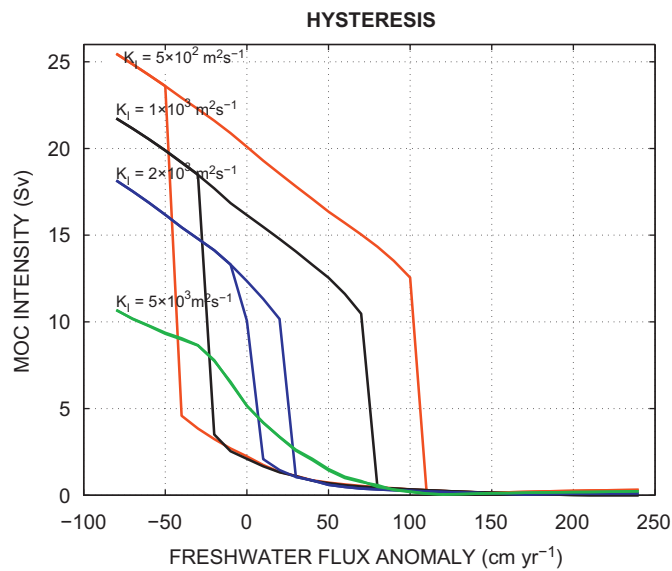
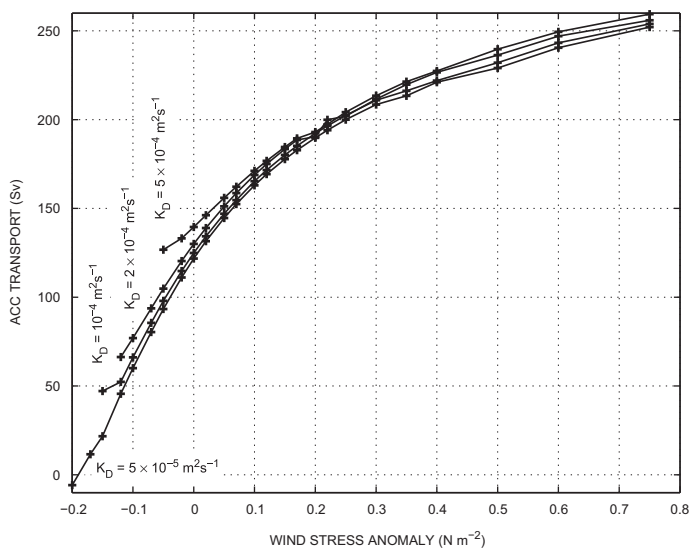


Fig. 15. AMOC hysteresis plots: overturning intensity as a function of anomalous freshwater flux \bar{F}_0 in the northern Atlantic for four values of isopycnal diffusivity: $K_i = 5 \times 10^2, 10^3, 2 \times 10^3, 5 \times 10^3 \text{ m}^2 \text{ s}^{-1}$. Note the disappearance of the hysteresis behavior for large K_i .



5. Conclusions

The AMOC is a critical component of the climate system important both for making future climate change projections and understanding past climate variations. In this study, to investigate the properties of the AMOC in a broad parameter range, we have formulated a new two-dimensional (latitude-depth) model of the ocean density structure and meridional overturning circulation.

The main difference of the present approach from previous zonally averaged models is a careful treatment of the processes in the Southern Ocean, including both the Eulerian-mean and eddy-induced flow (which comprise the residual mean circulation, see Marshall and Radko, 2006). Consequently, our model gives a proper representation of the Southern Ocean upwelling, the slope of the isopycnals in the Antarctic circumpolar channel and, implicitly, of the Antarctic Circumpolar Current (ACC).

We decompose the Eulerian-mean circulation into two components, the thermohaline and wind-driven, and also take into account the effects of diapycnal and isopycnal diffusion. The water that subducts in northern high latitudes is brought back to the surface either in the Southern Ocean (wind-driven upwelling) or throughout the ocean basin (mixing-driven upwelling). For the reference state of the model, the two upwelling processes are nearly equipartitioned in terms of their upward volume transport. Comprehensive ocean GCMs estimate the respective contributions of the two processes to the total upwelling in the range 40–60%, which puts our two-dimensional model just in the middle.

As criteria for assessing the realism of the model one can choose key characteristics of the mean ocean circulation, such as the strength of the North Atlantic overturning (16 Sv in the model), the depth of penetration of NADW (3000 m), the volume transport of the ACC through the Drake passage (125 Sv), the intensity of the Deacon cell in the Southern Ocean (26 Sv) and several others. It is actually surprising how quantitatively accurate this idealized model is, as compared to observations, for reproducing the mean state of the ocean circulation as well as ocean thermal and salinity structure (especially in the upper 1000 m of the ocean).

To test the sensitivity of the AMOC in our model, we conducted multiple experiments for a number of control parameters. These parameters are surface freshwater flux in the northern Atlantic, wind

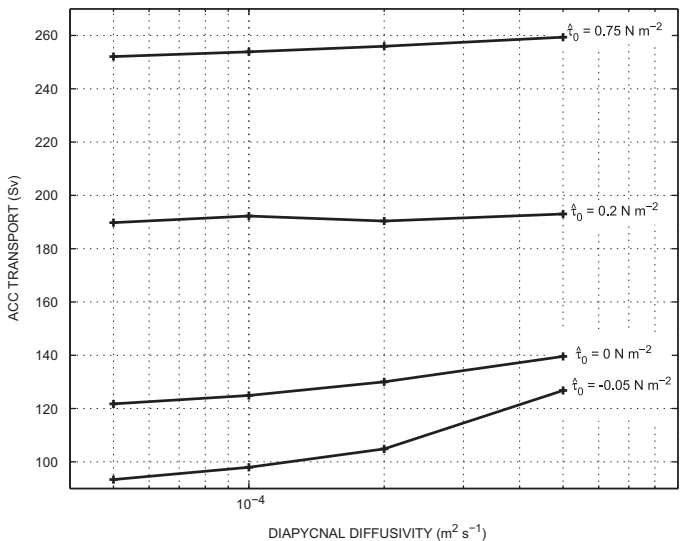


Fig. 16. (Left) The calculated zonal transport of the ACC as a function of anomalous wind stress $\bar{\tau}_0$ in the Southern Ocean (for the AMOC on-states) for four different values of diapycnal diffusivity. (Right) The ACC transport as a function of diapycnal diffusivity K_D for different wind stress anomalies in the Southern Ocean.

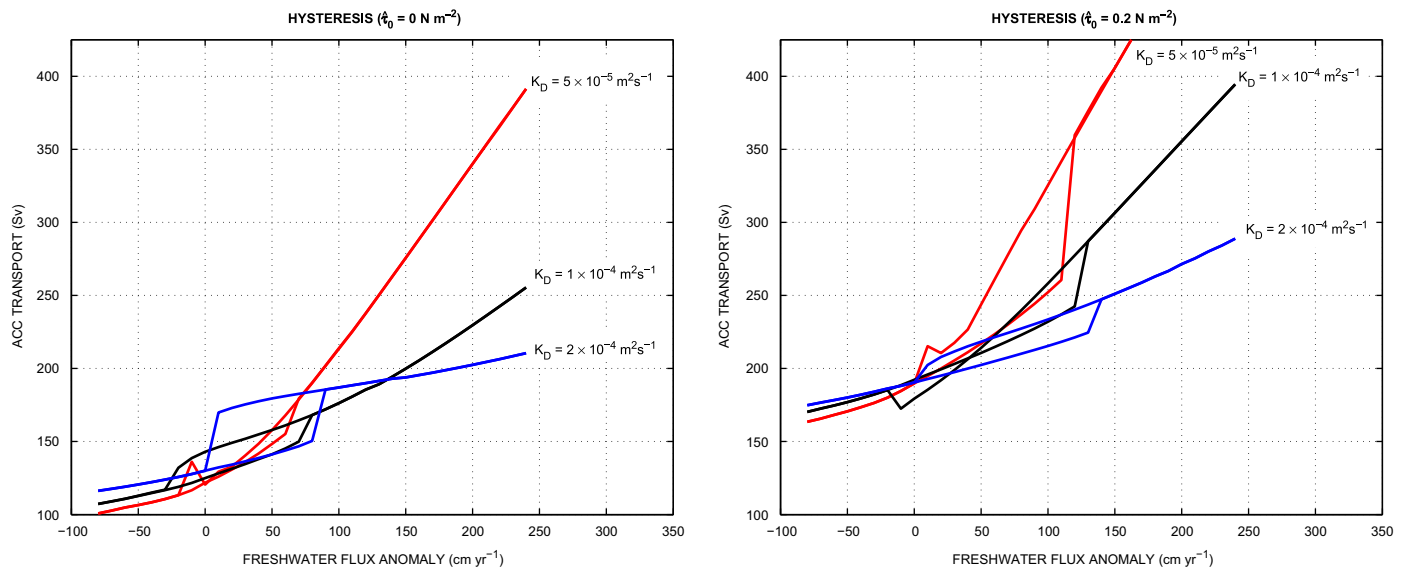


Fig. 17. The ACC volume transport as a function of anomalous freshwater flux $\hat{\mathcal{F}}_0$ imposed on the northern Atlantic (cf. Fig. 13) for two different wind stress anomalies (left: $\hat{\tau}_0=0$, right: $\hat{\tau}_0=+0.2 \text{ N m}^{-2}$). Each series of experiments is repeated for three values of diapycnal diffusivity $K_D=5 \times 10^{-5}$, 10^{-4} , $2 \times 10^{-4} \text{ m}^2 \text{ s}^{-1}$. Note the hysteresis loops in which the ACC transport has two possible values corresponding to the on- and off-states of the AMOC (the lower and upper branches of the hysteresis loops, respectively).

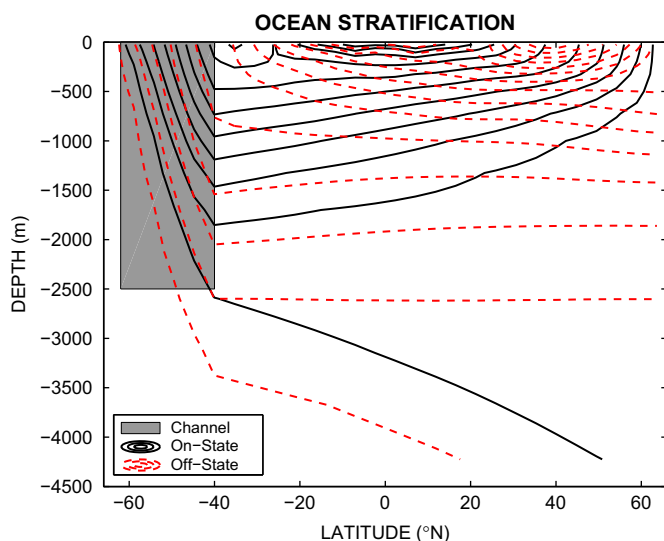


Fig. 18. Ocean stratification as a function of latitude and depth for the on- and off-states of AMOC (black solid and red dashed lines, respectively) for reference ocean conditions. Isopycnal surfaces are shown with a contour interval of 0.5 kg m^{-3} . The deepest isopycnals correspond to the potential density surfaces of $\rho = 1027.5$ and 1028 kg m^{-3} for the on- and off-states, respectively.

stress in the Southern Ocean, and diapycnal diffusivity (additional experiments were conducted with changes in the model isopycnal diffusivity). It is an interplay between these parameters that controls the AMOC strength and its stability characteristics such as the magnitude of forcing needed for the AMOC collapse (as seen from the general stability maps in Fig. 14).

As expected, larger values of diapycnal diffusivity, a stronger wind stress, and weaker freshwater fluxes lead to greater overturning. In particular, the dependence of the AMOC on diapycnal diffusivity in the model is nearly $K_D^{1/2}$ (in a broader parameter range the power of K_D vary from $1/3$ to $2/3$). Also, the sensitivity of the AMOC in the parameter range close to the reference conditions is roughly 1 Sv per 20% increase in the wind stress, and -0.7 Sv for a 10 cm yr^{-1} increase in freshwater fluxes.

The estimated volume transport of the ACC follows approximately the logarithmic law as a function of the total wind stress in the circumpolar channel. While Ekman transport is directly proportional to the wind stress, the zonal velocity in the ACC is related to the slope of the isopycnals, which is determined by a competition between the northward Ekman transport and the southward eddy-induced advection in the circumpolar channel.

We also find a moderate dependence of the ACC transport on diapycnal diffusion (we see a roughly 20% increase in the ACC transport per order-of-magnitude increase in diapycnal diffusivity over the ocean basin). This transport also increases when freshwater fluxes are imposed on the northern high latitudes. These two effects are related to deepening of the ocean thermocline which causes a subsequent adjustment of ocean stratification in the circumpolar channel and an increase in the isopycnal's slope.

Further, our experiments confirm the existence of the well-known hysteresis behavior associated with changes in freshwater fluxes. The hysteresis corresponds to the existence of a bistable regime (i.e. two different stable steady states can exist for the same combination of control parameters). As a new result, we show that a similar hysteresis behavior emerges when the system experiences gradual changes in the wind stress over the Southern Ocean.

In the bistable regime one steady state corresponds to the present-day ocean circulation and stratification (the AMOC on-state), the other corresponds to a collapsed AMOC (the off-state). For the latter state, the North Atlantic basin becomes filled with waters coming from the South Ocean: the AAIW and the AABW. Ocean vertical stratification becomes much stronger in the North Atlantic, but weaker in the South Atlantic. Isopycnal surfaces throughout the ocean become virtually flat for the off-state except in the Southern Ocean (Fig. 18). The depth of isopycnal surfaces is now controlled by a balance between the effect of the circumpolar channel and that of the uniform diapycnal mixing.

The size of the hysteresis loop, and thus the extent of the bistable regime, is controlled, in a complicated matter by the two parameters responsible for ocean upwelling: wind stress over the Southern Ocean and diapycnal diffusivity. It is significant that the height (difference in the AMOC strengths between the lower and upper branches) and the width of the hysteresis loop (the extent of the bistable regime) can be affected differently by these parameters. For example, an increase in

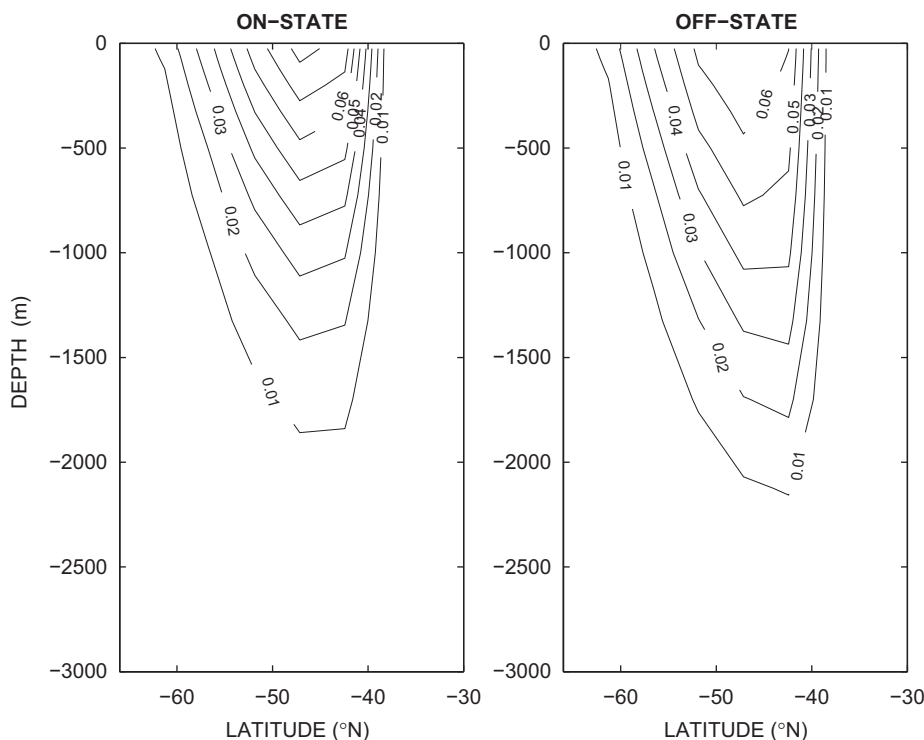


Fig. 19. Mean zonal velocity (m s^{-1}) in the ACC as a function of latitude and depth for the on- and off-states of the AMOC (the left and right panels, respectively) corresponding to the ocean stratification shown in Fig. 18. Note a deeper penetration of the ACC into the ocean for the off-state. Positive values indicate eastward flow.

diapycnal diffusivity in the model can lead to an increase in the height of the loop but a decrease in the width of the loop (Fig. 13). For low values of diapycnal diffusivity both the height and width of the loop decrease together, but it does not appear that the hysteresis loop disappears completely as a few other studies suggested (e.g. Prange et al., 2003). A potential reason for this discrepancy is a reduced role of the Southern Ocean upwelling in some of those studies. A related issue is the representation of mixing by horizontal/vertical diffusion, rather than isopycnal/diapycnal diffusion as done in our work, which is particularly important in the Southern Ocean.

Additional numerical experiments show that the hysteresis disappears in our model when isopycnal diffusivity is increased. Presumably, it is related to the reduction in density gradients in the ocean by excessive horizontal mixing. It is possible that a failure of some coupled models to show the hysteresis behavior can be related to this issue.

Another important result of this work is related to changes in the ACC volume transport between the two ocean states. We show that when the AMOC collapses, the ACC transport increases by almost 20 Sv in the model! It would be interesting to look in the paleorecords to see whether such a change indeed happened during previous reorganizations of the AMOC (e.g. McManus et al., 2004).

Future continuation of this work will include the coupling of the ocean model to (1) a simple atmospheric model and (2) a simple ice model to get a better representation of the sensitivity of the AMOC. It will be important to explore how atmosphere- and ice-ocean interactions modify the hysteresis behavior and the overall sensitivity of the AMOC to external forcing. It will be also important to test if the new system is able to generate quick transitions between the two steady states as an internal mode of climate variability.

Acknowledgments

This research was supported by grants from NSF (OCE-0901921), DOE Office of Science (DE-FG02-08ER64590), and the

The David and Lucile Packard Foundation. A.V.F. thanks David Marshall for a helpful discussion.

References

- Alley, R.B., et al., 2003. Abrupt climate change. *Science* 299, 2005–2010.
- Barreiro, M., et al., 2008. Abrupt climate changes: how freshening of the Northern Atlantic affects the thermohaline and wind-driven oceanic circulations. *Rev. Earth Planet. Sci.* 36, 33–58.
- Boccaletti, G., et al., 2004. The thermal structure of the upper ocean. *J. Phys. Oceanogr.* 34, 888–902.
- Broecker, W.S., 1990. Salinity history of the northern Atlantic during the last deglaciation. *Paleoceanography* 5, 459–467.
- Broecker, W.S., 1991. The great ocean conveyor. *Oceanography* 4, 79–89.
- Broecker, W.S., 2003. Does the trigger for abrupt climate change reside in the ocean or in the atmosphere? *Science* 6, 1519–1522.
- Bryden, H.L., Cunningham, S.A., 2003. How wind-forcing and air-sea heat exchange determine the meridional temperature gradient and stratification for the Antarctic circumpolar current. *J. Geophys. Res.* 108, C001296.
- Clarke, G., et al., 2003. Superlakes, megafloods and abrupt climate change. *Science* 301, 922–923.
- Curry, R., Dickson, B., Yashayaev, I., 2003. A change in freshwater balance of the Atlantic ocean over the past four decades. *Nature* 426, 826–829.
- Curry, R., Mauritzen, C., 2005. Dilution of the northern North Atlantic ocean in recent decades. *Science* 308, 1772–1774.
- Dickson, B., et al., 2002. Rapid freshening of the deep North Atlantic ocean over the past four decades. *Nature* 416, 832–837.
- Dijkstra, H.A., 2007. Characterization of the multiple equilibria regime in a global ocean model. *J. Climate* 59A, 695–705.
- Dijkstra, H.A., 2008. Scaling of the Atlantic meridional overturning circulation in a global ocean model. *J. Climate* 60A, 749–760.
- Dijkstra, H.A., Weijer, W., 2003. Stability of the global ocean circulation: the connection of equilibria within a hierarchy of models. *J. Mar. Res.* 61, 725–743.
- Drbohlav, J., Jin, F.F., 1998. Interdecadal variability in a zonally averaged ocean model: an adjustment oscillator. *J. Phys. Oceanogr.* 28, 1252–1270.
- Ekstrom, G., Nettles, M., Tsai, V.C., 2006. Seasonality and increasing frequency of Greenland glacial earthquakes. *Science* 311, 1756–1758.
- Fedorov, A.V., et al., 2004. The effect of salinity on the wind-driven circulation and the thermal structure of the upper ocean. *J. Phys. Oceanogr.* 34, 1949–1966.
- Fedorov, A.V., et al., 2007. The freshening of surface waters in high latitudes: effects on the thermohaline and wind-driven circulations. *J. Phys. Oceanogr.* 37, 896–907.
- Gagosian, R.B., 2003. Abrupt climate change, should we be worried? *Woods Hole Oceanographic Institution, World Economic Forum*, pp. 1–15.

- Ganachaud, A., Wunsch, C., 2000. Improved estimates of global ocean circulation, heat transport and mixing from hydrographic data. *Nature* 408, 453–457.
- Ganopolski, A., Rahmstorf, S., 2001. Rapid changes of glacial climate simulated in a coupled climate model. *Nature* 409, 153–158.
- Gent, P.R., McWilliams, J.C., 1990. Isopycnal mixing in ocean circulation model. *J. Phys. Oceanogr.* 20, 150–155.
- Gnanadesikan, A., 1999. A simple predictive model for the structure of the oceanic pycnocline. *Science* 283, 2077–2079.
- Gnanadesikan, A., de Boer, A.M., Mignone, B.K., 2007. A simple theory of the pycnocline and overturning revisited. Past and future changes of the ocean's meridional overturning circulation. *Geophysical Monograph*, vol. 173, pp. 19–32.
- Griffies, S.M., et al., 2009. Coordinated ocean-ice reference experiments (COREs). *Ocean Modell.* 26, 1–46.
- Hirabara, M., Ishizaki, H., Ishikawa, I., 2007. Effects of the wind stress over the southern ocean on the meridional overturning. *J. Phys. Oceanogr.* 37, 2114–2132.
- Hofmann, M., Rahmstorf, S., 2009. On the stability of the Atlantic meridional overturning circulation. *Proc. Natl. Acad. Sci. USA* 106, 20584–20589.
- IPCC, 2007. *Climate Change 2007—The Physical Science Basis: Contribution of Working Group I to the Fourth Assessment Report of the IPCC*. Cambridge University Press, Cambridge.
- Josey, S.A., Marsh, R., 2005. Surface freshwater flux variability and recent freshening of the North Atlantic in the eastern subpolar gyre. *J. Geophys. Res.* 110, C05008.
- Kamenkovich, I.V., Sarachik, E.S., 2004. Mechanisms controlling the sensitivity of the Atlantic thermohaline circulation to the parameterization of eddy transports in an ocean GCM. *J. Phys. Oceanogr.* 34, 1628–1647.
- Liu, Z., et al., 2009. Transient simulation of last deglaciation with a new mechanism for Bølling–Allerød warming. *Science* 17, 310–314.
- Lynch-Stieglitz, J., et al., 2007. Atlantic overturning circulation during the last glacial maximum. *Science* 316, 66–69.
- Manabe, S., Stouffer, R.J., 1995. Simulation of abrupt climate change induced by freshwater input by freshwater input to the North Atlantic. *Nature* 378, 165–167.
- Manabe, S., Stouffer, R.J., 1999. The role of thermohaline circulation in climate. *J. Climate* 51A, 91–109.
- Marchal, O., et al., 2007. Buoyancy-driven flow and nature of vertical mixing in a zonally averaged model. *Geophys. Monogr. Ser.* 173, 33–52.
- Marotzke, J., 1991. Influence of convective adjustment on the stability of the thermohaline circulation. *J. Phys. Oceanogr.* 21, 903–907.
- Marotzke, J., Welander, P., Willebrand, J., 1988. Instability and multiple steady states in a meridional-plane model of the thermohaline circulation. *J. Climate* 40A, 162–172.
- Marotzke, J., Willebrand, J., 1991. Multiple equilibria of the global thermohaline circulation. *J. Phys. Oceanogr.* 21, 1372–1385.
- Marshall, J., Radko, T., 2003. Residual mean solutions for the Antarctic Circumpolar Current and its associated overturning circulation. *J. Phys. Oceanogr.* 33, 2341–2354.
- Marshall, J., Radko, T., 2006. A model of the upper branch of the meridional overturning of the southern ocean. *Prog. Oceanogr.* 70, 331–345.
- McCreary Jr., J.P., Lu, P., 1994. Interaction between the subtropical and equatorial ocean circulations: the subtropical cell. *J. Phys. Oceanogr.* 24, 466–497.
- McManus, J.F., et al., 2004. Collapse and rapid resumption of Atlantic meridional circulation linked to deglacial climate changes. *Nature* 428, 834–836.
- Mignot, J., Levermann, A., Griesel, A., 2006. A decomposition of the Atlantic meridional overturning circulation into physical components using its sensitivity to vertical diffusivity. *J. Phys. Oceanogr.* 20, 636–650.
- Munk, W.H., 1950. On the wind driven ocean circulation. *J. Meteorol.* 7, 79–93.
- Nof, D., Van Gordera, S., de Boer, A., 2007. Does the Atlantic meridional overturning cell really have more than one stable steady state? *Deep-Sea Res.* 54, 2005–2021.
- Orsi, A.H., Whitworth, T., Nowlin, W.D., 1995. On the meridional extent and fronts of the Antarctic circumpolar current. *Deep-Sea Res.* 42, 641–673.
- Paillard, D., Cortijo, E., 1999. A simulation of the Atlantic meridional circulation during Heinrich event 4 using reconstructed sea surface temperatures and salinity. *Paleoceanography* 14, 716–724.
- Park, Y.-G., Bryan, K., 2000. Comparison of thermally driven circulations from a depth-coordinate model and an isopycnal-layer model. Part I: scaling-law sensitivity to vertical diffusivity. *J. Phys. Oceanogr.* 30, 590–605.
- Peterson, R.G., 1988. On the transport of the Antarctic circumpolar current through drake passage and its relation to wind. *J. Geophys. Res.* 93, 993–1004.
- Prange, M., Lohmann, G., Paul, A., 2003. Influence of vertical mixing on the thermohaline hysteresis: analyses of an OGCM. *J. Phys. Oceanogr.* 33, 1707–1721.
- Rahmstorf, S., 1995. Bifurcation of the Atlantic thermohaline circulation in response to changes in the hydrological cycle. *Nature* 378, 145–149.
- Rahmstorf, S., 2000. The thermohaline ocean circulation—a system with dangerous threshold? *Clim. Change* 46, 247–256.
- Rahmstorf, S., 2002. Ocean circulation and climate during the past 120,000 years. *Nature* 419, 207–214.
- Rahmstorf, S., 2006. Thermohaline ocean circulation. In: Elias, S.A. (Ed.), *Encyclopedia of Quaternary Sciences*. Elsevier, Amsterdam.
- Rahmstorf, S., et al., 2005. Thermohaline circulation hysteresis: a model inter-comparison. *Geophys. Res. Lett.* 32, L23605.
- Redi, M.H., 1982. Oceanic isopycnal mixing by coordinate rotation. *J. Phys. Oceanogr.* 12, 1154–1158.
- Rind, D., et al., 2001. Effect of glacial meltwater in GISS coupled atmosphere-ocean model. 1. North Atlantic deep water response. *J. Geophys. Res.* 106, 27335–27353.
- Sakai, K., Peltier, W.R., 1995. A simple model of the Atlantic thermohaline circulation: internal and forced variability with paleoclimatological implications. *J. Geophys. Res.* 100, C00616.
- Schmittner, G.A., Weaver, A.J., 2001. Dependence of multiple climate states on ocean mixing parameters. *Geophys. Res. Lett.* 28, 1027–1030.
- Sévellec, F., Huck, T., Ben Jelloul, M., 2006. On the mechanism of centennial thermohaline oscillations. *J. Mar. Res.* 64, 355–392.
- Speer, K., Rintoul, S.R., Sloyan, B., 2000. The diabatic deacon cell. *J. Phys. Oceanogr.* 30, 3212–3222.
- Stocker, T.F., Mysak, L.A., 1992. Climatic fluctuations on the century time scale: a review of high-resolution proxy data and possible mechanisms. *Clim. Change* 20, 227–250.
- Stommel, H., 1948. The westward intensification of wind-driven ocean currents. *Trans. Am. Geophys. Union* 29, 202–206.
- Stommel, H., 1958. The abyssal circulation. *Deep-Sea Res.* 4, 80–82.
- Stommel, H., 1961. Thermohaline convection with stable regimes flow. *J. Climate* 13, 224–230.
- Stommel, H., Arons, A.B., 1960a. On the abyssal circulation of the world ocean—I. Stationary planetary flow patterns on a sphere. *Deep-Sea Res.* 6, 140–154.
- Stommel, H., Arons, A.B., 1960b. On the abyssal circulation of the world ocean—II. An idealized model of the circulation pattern and amplitude in oceanic basins. *Deep-Sea Res.* 6, 217–233.
- Stouffer, R.J., et al., 2006. Investigating the cause of the thermohaline circulation to past and future climate changes. *J. Climate* 19, 698–722.
- Sverdrup, H.P., 1947. Wind-driven currents in a baroclinic ocean; with application to the equatorial current of eastern Pacific. *Proc. Natl. Acad. Sci. USA* 33, 318–326.
- Talley, L.D., Pickard, G.L., Emery, W.J., Swift, J.H., 2011. *Descriptive Physical Oceanography: An Introduction*. sixth ed. Elsevier, 600pp.
- Tansley, C.E., Marshall, D.P., 2001. On the dynamics of wind-driven circumpolar currents. *J. Phys. Oceanogr.* 31, 3258–3273.
- Toggweiler, J.R., Samuels, B., 1995. Effect of Drake passage on the global thermohaline circulation. *Deep-Sea Res.* 42, 477–500.
- Vallis, G.K., 2000. Large-scale circulation and production of stratification: effects of wind, geometry, and diffusion. *J. Phys. Oceanogr.* 30, 933–954.
- Vallis, G.K., 2006. *Atmospheric and Oceanic Fluid Dynamics*. Cambridge University Press.
- Vellinga, M., Wood, R.A., 2002. Global climatic impacts of a collapse of the Atlantic thermohaline circulation. *Clim. Change* 54, 251–267.
- Weaver, A.J., Sarachik, E.S., 1991. The role of mixed boundary conditions in numerical models of ocean's climate. *J. Phys. Oceanogr.* 21, 1470–1493.
- Weaver, A.J., Sarachik, E.S., Marotzke, J., 1991. Freshwater flux forcing of decadal and interdecadal oceanic variability. *Nature* 353, 836–838.
- Weaver, A.J., et al., 1993. Stability and variability of the thermohaline circulation. *J. Phys. Oceanogr.* 23, 39–60.
- Weijer, W., et al., 2003. A fully-implicit model of the global ocean circulation. *J. Comput. Phys.* 192, 452–470.
- Whitworth III, T., 1983. Monitoring the transport of the Antarctic Circumpolar Current at Drake Passage. *J. Phys. Oceanogr.* 13, 2045–2057.
- Wright, D.G., Stocker, T.F., 1991. A zonally averaged ocean model for thermohaline circulation. Part I: model development and flow dynamics. *J. Phys. Oceanogr.* 21, 1713–1724.
- Wright, D.G., Stocker, T.F., 1992. Sensitivities of a zonally averaged global ocean circulation model. *J. Geophys. Res.* 97, 12707–12730.
- Wright, D.G., Stocker, T.F., Mercer, D., 1998. Closures used in zonally averaged ocean models. *J. Phys. Oceanogr.* 28, 791–804.
- Wright, D.G., Vreugdenhil, C.B., Hughes, T.M., 1995. Vorticity dynamics and zonally averaged ocean circulation models. *J. Phys. Oceanogr.* 25, 2141–2154.
- Wunsch, C., Ferrari, R., 2004. Vertical mixing, energy, and the general circulation of the oceans. *Annu. Rev. Fluid Mech.* 36, 281–314.
- Zhang, J., Schmitt, R.W., Huang, R.X., 1999. The relative influence of diapycnal mixing and hydrologic forcing on the stability of the thermohaline circulation. *J. Phys. Oceanogr.* 29, 1096–1108.
- Zhang, R., Delworth, T., 2005. Simulated tropical response to a substantial weakening of the Atlantic thermohaline circulation. *J. Climate* 18, 1853–1860.